

# Non-linear states in parallel Blasius boundary layer

M U H A M M E D   A B D U L L A H   A L   A H A D

Master of Science Thesis  
Stockholm, Sweden 2014



# Non-linear states in parallel Blasius boundary layer

M U H A M M E D   A B D U L L A H   A L   A H A D

Master's Thesis in Scientific Computing (30 ECTS credits)  
Master Programme in Scientific Computing (120 credits)  
Royal Institute of Technology year 2014  
Supervisor at KTH was Philipp Schlatter  
Examiner was Michael Hanke

TRITA-MAT-E 2014: 66  
ISRN-KTH/MAT/E--14/66--SE

Royal Institute of Technology  
*School of Engineering Sciences*

**KTH** SCI  
SE-100 44 Stockholm, Sweden

URL: [www.kth.se/sci](http://www.kth.se/sci)



# Abstract

There is large theoretical, experimental and numerical interest in studying boundary layers, which develop around any body moving through a fluid. The simplest of these boundary layers lead to the theoretical abstraction of a so-called Blasius boundary layer, which can be derived under the assumption of a flat plate and zero external pressure gradient. The Blasius solution is characterised by a slow growth of the boundary layer in the streamwise direction. For practical purposes, in particular related to studying transition scenarios, non-linear finite-amplitude states (exact coherent states, edge states), but also for turbulence, a major simplification of the problem could be attained by removing this slow streamwise growth, and instead consider a parallel boundary layer. Parallel boundary layers are found in reality, e.g. when applying suction (asymptotic suction boundary layer) or rotation (Ekman boundary layer), but not in the Blasius case. As this is only a model which is not an exact solution to the Navier-Stokes (or boundary-layer) equations, some modifications have to be introduced into the governing equations in order for such an approach to be feasible. Spalart and Yang introduced a modification term to the governing Navier-Stokes equations in 1987. In this thesis work, we adapted the amplitude of the modification term introduced by Spalart and Yang to identify the nonlinear states in the parallel Blasius boundary layer. A final application of this modification was in determining the so-called edge states for boundary layers, previously found in the asymptotic suction boundary layer.



# Referat

## Icke-linjära stater i parallell Blasius gränsskikt

Det finns stor teoretisk, experimentell och numerisk intresse för att studera gränsskikt som utvecklas runt varje kropp som rör sig genom en vätska. Det enklaste av detta gränsskikt leder till den teoretiska abstraktion av ett s.k. Blasius gränsskikt, som kan härledas under antagande av en plan platta utan externt tryckgradient. Blasius lösningen karakteriseras av en långsam tillväxt av gränsskiktet i strömningsriktningen. Av praktiska skäl, särskilt i samband med att studera övergångsscenarier, icke-linjära finita-amplitud tillstånd ("exact coherent state" på engelska), men även för turbulens, en stor förenkling av problemet kan nås genom att ta bort denna långsamma strömväxt, och istället överväga en parallell gränsskikt. Parallella gränsskikt finns i verkligheten, t.ex. vid sugning (asymptotisk sugningsgränsskiktet) eller rotation (Ekman gränsskiktet), men inte i Blasius fallet. Eftersom detta är bara en modell som inte är en exakt lösning på Navier-Stokes (eller gränsskiktets) ekvationer, vissa ändringar måste införas i de styrande ekvationer för att en sådan strategi ska vara genomförbart. Spalart och Yang infört en enkel ändring i Navier-Stokes ekvationer redan 1987. I detta examensarbete har vi anpassat amplituden av modifieringstermen att identifiera de icke-linjära tillstånd i det parallella Blasius gränsskiktet. Motivation av tillämpning av denna ändring var att fastställa de så kallade "edge states" för gränsskikt, som tidigare har hittats i det asymptotiska sugningsgränsskiktet.



## **Acknowledgements**

My first and foremost thanks goes to my supervisor Dr. Philipp Schlatter for his continuous advice and guidance throughout the thesis work. I am extremely grateful to him for sharing his knowledge and ideas with me.

I would also like to thank my co-supervisor Taras Khapko, Ph.D student at KTH Mechanics for his invaluable help and discussions on every aspects of the thesis work.

Finally, I would like to thank my family and friends for their support and encouragement.



# Contents

<b>List of Figures</b>	<b>2</b>
<b>1 Introduction</b>	<b>3</b>
<b>2 Governing Equations</b>	<b>7</b>
2.1 Incompressible Navier-Stokes Equations . . . . .	7
2.2 Boundary-layer equations . . . . .	8
2.2.1 Blasius solutions to the boundary layer on a flat plate . . . . .	8
<b>3 Theory</b>	<b>11</b>
3.1 Forcing . . . . .	11
3.1.1 Spalart and Yang method . . . . .	13
3.1.2 Wedin <i>et al</i> study . . . . .	14
3.1.3 Present study . . . . .	15
3.1.4 Forcing profile . . . . .	16
3.2 Boundary conditions . . . . .	16
<b>4 Numerical Method</b>	<b>19</b>
4.1 Temporal discretization . . . . .	19
4.2 Space discretization: Horizontal direction . . . . .	20
4.3 Space discretization: Normal direction . . . . .	20
4.4 Properties of the discretizations . . . . .	20
4.5 Edge tracking . . . . .	22
<b>5 Validation and results</b>	<b>25</b>
5.1 2D . . . . .	25
5.2 3D . . . . .	33
5.3 Edge state . . . . .	47
<b>6 Conclusion and future work</b>	<b>51</b>
<b>Bibliography</b>	<b>53</b>



# List of Figures

2.1	Blasius similarity solutions of the boundary-layer equations . . . . .	9
3.1	Effect of forcing in the boundary-layer flow, $\delta^*$ vs $t$ . . . . .	12
3.2	Effect of forcing in the boundary-layer flow, $U/U_\infty$ vs $y$ . . . . .	12
3.3	Forcing profile . . . . .	16
4.1	The absolute stability regions . . . . .	22
4.2	Conceptual sketch of the edge-tracking algorithm . . . . .	23
5.1	Validating results with Spalart and Yang method for $Re_{\delta^*} = 510$ in 2D case	26
5.2	Validating results with Spalart and Yang method for $Re_{\delta^*} = 600$ in 2D case	27
5.3	Mean velocity profile for $Re_{\delta^*} = 510, 600$ in 2D case . . . . .	28
5.4	$u_{tot}^{00}(y_{max})$ mode and amplitude of the forcing for $Re_{\delta^*} = 510, 600, 1000$ in 2D for the present method . . . . .	29
5.5	TS wave travelling in the flow in 2D case . . . . .	30
5.6	Increase of TS waves amplitude in 2D case . . . . .	31
5.7	Norm of the difference of the solution of two methods in 2D case . . . . .	32
5.8	Comparing the results with Spalart and Yang for $Re_{\delta^*} = 500$ in a 3D domain	33
5.9	Mean-velocity profile for $Re_{\delta^*} = 500$ in 3D case . . . . .	34
5.10	TS waves in 3D for $Re_{\delta^*} = 500$ . . . . .	35
5.11	Shape factor $H$ for $Re_{\delta^*} = 500$ in 3D . . . . .	36
5.12	Validating results with Spalart and Yang for $Re_{\delta^*} = 1000$ in 3D . . . . .	37
5.13	Mean-velocity profile using wall variables in 3D for $Re_{\delta^*} = 1000$ . . . . .	38
5.14	Turbulent intensities in 3D for $Re_{\delta^*} = 1000$ in wall units, $u_{rms}^+$ vs $y^+$ and $v_{rms}^+$ vs $y^+$ . . . . .	39
5.15	Turbulent intensities in 3D for $Re_{\delta^*} = 1000$ in wall units, $w_{rms}^+$ vs $y^+$ and $(uv)_{rms}^+$ vs $y^+$ . . . . .	39
5.16	Visualization of the flow field for $Re_{\delta^*} = 1000$ in 3D, $xy$ -contour plot of $u$ .	40
5.17	Visualization of the flow field for $Re_{\delta^*} = 1000$ in 3D, $xy$ -contour plot of $v$ .	41
5.18	$v$ vs $y$ for $Re_{\delta^*} = 1000$ at five different point of $x$ and $z = 0$ . . . . .	43
5.19	$u$ vs $x$ for $Re_{\delta^*} = 1000$ at five different point of $y$ and $z = 0$ . . . . .	44
5.20	Turbulence structures near the wall in 3D case . . . . .	46
5.21	$v_{rms}$ for $Re_{\delta^*} = 500$ in case of edge state . . . . .	47
5.22	Mean velocity at $y_{max}$ for $Re_{\delta^*} = 500$ in case of edge state . . . . .	48
5.23	Three-dimensional visualization of the laminar-turbulent separatrix, present results . . . . .	49



# Chapter 1

## Introduction

We experience flows in all fields of our natural and technical environment. The one that every living person at least experiences is the supply of oxygen in their body through the flow-dependent transport process. Our life on earth would have been different or even impossible without fluid flows. Our natural and technological world could have been perished without it.

Understanding the fluid flow-related phenomena is a long standing subject of research both for academic and industrial purposes. Flows are typically categorized as two different phenomena known as laminar and turbulent flow. If a dye is injected in the middle of stream of free flowing water through a pipe, the resulting flow could be either laminar or turbulent. Osbourne Reynolds (1842-1912) was the first person to investigate this phenomenon in the 1880s, later became a classics in fluid mechanics [16].

After many experiments he found that the expression  $\rho u d / \mu$ , where  $\rho$  = density,  $u$  = mean velocity,  $d$  = diameter of the pipe and  $\mu$  = viscosity, would help to predict what the flow behavior could be. Value less than 2000 result in laminar flow where the motion of the particles of the fluid is very orderly distributed and all particles moves in straight lines parallel to the pipe walls. Whereas the flow become irregular in space and time for value greater than 4000, known as turbulent flow. This number expressed by  $\rho u d / \mu$  later named as Reynolds number,  $Re$ . Reynolds also observed another type of flow in between laminar and turbulent flow for the range  $2000 < Re < 4000$  defined as transitional flow [16].

Ever since the pioneering experimental study on pipe flows by Reynolds, there has been decades of effort to get fundamental insight how a flow undergoes transition from laminar to turbulent. But still our ability to answer the question of how a turbulent flow arises and sustains is far from satisfactory. We can observe turbulent or transitional state in many technical applications such as flow over an airplane wings or around a car body. Hence, understanding turbulence and transitional flow is of great significance. Controlling transition could allow significant improvement in many applications. For example, by delaying transition skin-friction drag can be reduced in case of flow over a airplane wings and thus smaller fuel consumptions can be achieved. On the other hand, allowing transition to turbulence, mixing for combustion, heat transfer, chemical reaction and other exchange processes can be enhanced.

Viscosity, how viscous a fluid is, is one of the important physical parameters of a fluid that defines how the fluid flow will behave. All solid surfaces interact with viscous fluid because of the no-slip boundary condition. The physical requirement is that the fluid and solid have equal velocities at their interface. Thus a boundary layer is formed when a viscous fluid moves over a solid surface as the flow is retarded by the fixed solid surface and the flow is termed as boundary-layer flow. In the present study we are going to deal with the simplest possible boundary layer that formed over a semi-infinite flat plate known as Blasius boundary layer. The boundary-layer flow on a flat plate is of great fundamental as well as practical importance.

A boundary-layer flow can be formulated in two possible ways, spatial and temporal. In spatial simulations a physical boundary layer usually develops in the downstream direction, while in case of temporal simulations boundary layer develops in time. A spatial formulation of a physical boundary layer is the best numerical model, but spatial development of inhomogeneous boundary layer makes it computationally demanding. Moreover, in turbulent flows the range of dynamically-significant length and time scales widens rapidly, hence making an accurate numerical solution increasingly costly. In this study we are going to use a model with periodic boundary conditions in the stream-wise and spanwise directions. There are several advantages of using periodic boundary conditions: very efficient Fourier spectral methods can be used, and, there are no inflow and outflow boundary conditions to be prescribed. In case of spatially growing boundary-layer flow a fringe region downstream of the physical domain needs to be added to retain the advantages of the spectral Fourier decomposition, results in computationally demanding simulation. This motivates us to go for temporal advancement of the boundary-layer flow, where the boundary layer develops in time rather than in space.

Spalart used a temporal simulation technique to compute the development of a flat plate boundary layer at a Reynolds number  $Re_\theta = 1410$  [23]. Temporal simulation technique has been adopted for this particular study as well. The basis of the temporal simulation technique is based on the fact that a localized disturbance or wave of relatively short wavelength which travels downstream in a slowly growing boundary layer is surrounded by a slowly temporal growing boundary layer of almost constant thickness. That is the idea is to use the fact that both the boundary layer thickness and the turbulence energy level vary slowly as functions of  $x$ .

Spalart and Yang [24] performed a study in 1985 related to ribbon-induced transition in Blasius flow on the parallel boundary-layer flow approximation. To perform their study, they added a correction term to the Navier-Stokes equations so that the laminar solution has a Blasius profile. They studied the early three-dimensional stages of transition in the Blasius boundary layer by numerical solution of the Navier-Stokes equations. They numerically solved the full, time-dependent, three-dimensional Navier-Stokes equations in the half-space over a plane wall with Blasius boundary layer as the initial condition disturbed by a finite-amplitude, two-dimensional TS wave [detailed in CHAPTER 3] and low-amplitude, three-dimensional random noise. They observed rapid amplification of the three-dimensional components which leads to transition. The early nonlinear stage has also been the subject of recent experimental, theoretical, and numerical work by Thomas (1983) [34]; Kachanov & Levchenko (1984) [11]; Saric, Kozlov & Levchenko (1984) [27]; Craik (1971) [2]; Herbert (1984, 1985) [7] [8]; Wray & Hussaini (1980) [37] and Spalart (1984) [22]. Wedin *et al* [9] performed a study to locate a relevant nonlinear

solution in a parallel boundary-layer flow. They also reported finite amplitude coherent structures together with a preliminary analysis of their stability. Their study was based on the self-sustaining process originally described by Waleffe [36] which requires adding a body force to the Navier-Stokes equations. Wedin *et al* [9] adapted the magnitude of the body force based on the mean velocity at the outer edge of the domain in the context of the disturbance formulation.

Relevant and similar studies as Wedin *et al* [9] have been carried out by Milinazzo & Saffman (1985) [19]; Koch (1992) [14]; Rotenberry(1993) [26] and Ehrenstein & Rossi (1996) [5] discovering nonlinear two-dimensional solutions to the Blasius boundary-layer flow. In Koch (1992) [14] the prechaotic bifurcation behavior of the Blasius boundary-layer flow was studied using the parallel flow approximation followed up by a secondary stability analysis of the nonlinear solutions. Rotenberry (1993) [26] studied the stability of the flow over a flat plate to finite-amplitude disturbances and found that the minimum Reynolds number of the nonlinear Tollmein-Schlichting waves is about 510 slightly below the linear critical point 519.4. His result suggests that finite amplitude disturbances can initiate transition. To perform his study, Rotenberry used a model described by Milinazzo & Saffman (1985) [19]. Ehrenstein & Koch (1995) [4] performed a secondary analysis of the two-dimensional nonlinear equilibrium solutions with a hope to find a key to the transition mechanism and to clarify the bursting process. Koch *et al* (2000) [15] reported three-dimensional nonlinear equilibrium solutions for a flow over an infinite swept flat plate.

In the current thesis, we have studied the linear behavior of single two-dimensional TS waves followed by an early nonlinear stage, during which two-dimensional nonlinear effects become significant, such as the saturation of a TS wave. Finally, a strong nonlinear stage, which leads to the fully turbulent boundary layer, was studied in a three-dimensional domain followed by the understanding of the dynamics of laminar-turbulent separatrix known as edge state. In the edge state case our aim was to identify a relative attractor on the laminar-turbulent separatrix, the invariant phase-space region separating trajectories that relaminarize from those experiencing turbulent dynamics. This thesis work woes much to the previous work by Wedin *et al* [9] and Spalart & Yang (1985) [24].



## Chapter 2

# Governing Equations

### 2.1 Incompressible Navier-Stokes Equations

The motion of the fluid substances is described by the Navier-Stokes equations, named after Claude-Louis Navier and George Gabriel Stokes. The equations comprise the conservation of mass and momentum equations. The general dimensional form is read as:

$$\begin{aligned}\rho \frac{D\mathbf{u}}{Dt} + \nabla p - \mu \nabla^2 \mathbf{u} &= 0 \\ \frac{D\rho}{Dt} + \nabla \cdot (\rho \mathbf{u}) &= 0\end{aligned}\tag{2.1.1}$$

where  $\rho$  is density,  $p$  is pressure,  $\mathbf{u} = (u, v, w)$  are velocity components and  $\mu$  is the molecular viscosity.

The material derivative  $\frac{D}{Dt} = \frac{\partial}{\partial t} + \mathbf{u} \cdot \nabla$ , is the time rate of change of some fluid quantity from the viewpoint of Eulerian definition of fluid. In case of incompressible flow the density  $\rho$  is assumed to be constant, which leads us to  $\frac{D\rho}{Dt} \equiv \frac{\partial \rho}{\partial t} + \mathbf{u} \cdot \nabla \rho = 0$ .

Thus for incompressible flow the Navier-Stokes equation takes the form:

$$\begin{aligned}\mathbf{u}_t + \frac{1}{\rho} \nabla p - \nu \nabla^2 \mathbf{u} + (\mathbf{u} \cdot \nabla) \mathbf{u} &= 0 \\ \nabla \cdot \mathbf{u} &= 0\end{aligned}\tag{2.1.2}$$

where  $\nu = \frac{\mu}{\rho}$  is the dynamic viscosity.

The dimensional incompressible Navier-Stokes equations defined by (2.1.2) are non-dimensionalized based on unidirectional free-stream speed  $U_\infty$  and the displacement boundary-layer thickness,  $\delta^* = \int_{y=0}^{\infty} (1 - \frac{u}{U_\infty}) dy$ . The non-dimensional form of (2.1.2):

$$\begin{aligned}\mathbf{u}_t + \nabla p - \frac{1}{Re_{\delta^*}} \nabla^2 \mathbf{u} + (\mathbf{u} \cdot \nabla) \mathbf{u} &= 0 \\ \nabla \cdot \mathbf{u} &= 0\end{aligned}\tag{2.1.3}$$

where  $Re_{\delta^*} = \frac{U_\infty \delta^*}{\nu}$  is the Reynolds number based on the boundary-layer displacement thickness  $\delta^*$ .

## 2.2 Boundary-layer equations

The relevant equations for laminar boundary-layer flow is one of the most important advances in fluid dynamics which is based on few assumptions. One of the assumption is that  $Re_{\delta^*} = \frac{U_{\infty}\delta^*}{\nu} \rightarrow \infty$ . This assumption along with using an order of magnitude analysis of the Navier-Stokes equations of the viscous flow, help to decide which terms are important and which terms are less important to be negligible to simplify the solutions of equations within the boundary layer. The dimensionless two-dimensional simplified boundary-layer equations for streamwise and normal velocity components  $u$  and  $v$  can be written as :

$$\begin{aligned} \frac{\partial u}{\partial x} + \frac{\partial v}{\partial y} &= 0 \\ u \frac{\partial u}{\partial x} + v \frac{\partial u}{\partial y} &= -\frac{\partial p}{\partial x} + \frac{1}{Re_{\delta^*}} \frac{\partial^2 u}{\partial y^2} \\ 0 &= \frac{\partial p}{\partial y} \end{aligned} \quad (2.2.1)$$

The assumption of high Reynolds number divide the flow over a surface into a region unaffected by the viscosity known as outer region and a near surface region where the viscous effect can not be neglected known as boundary layer. The asymptotic analysis in the boundary-layer equations states that the contribution from the wall-normal velocity component  $v$  is small compared with the streamwise velocity component  $u$ , and also that the variations of any fluid properties is much smaller in the streamwise direction than that of the normal direction, i.e  $\frac{\partial}{\partial x} \ll \frac{\partial}{\partial y}$ . It is also worthy to note that the boundary-layer approximation is not valid near the leading edge  $x = 0$  of the domain since the assumption  $Re_{\delta^*} \gg 1$  and  $\frac{\partial}{\partial x} \ll \frac{\partial}{\partial y}$  are incorrect there. According to the study [20] the boundary-layer approximation is valid for Reynolds number above 30.

### 2.2.1 Blasius solutions to the boundary layer on a flat plate

For constant free-stream flow velocity  $U_{\infty}$  and external zero pressure gradient  $\frac{\partial p}{\partial x} = 0$ , we observe the simplest possible steady two-dimensional boundary layer forms on a semi-infinite flat plate at zero angle of incidence known as Blasius boundary layer. In this special case the non-dimensionalized boundary-layer equations simplify to:

$$\begin{aligned} \frac{\partial u}{\partial x} + \frac{\partial v}{\partial y} &= 0 \\ u \frac{\partial u}{\partial x} + v \frac{\partial u}{\partial y} &= \frac{1}{Re_{\delta^*}} \frac{\partial^2 u}{\partial y^2} \end{aligned} \quad (2.2.2)$$

The solution of the equations (2.2.2) should be valid for any values of  $x$  except for the leading edge  $x = 0$ . Hence the corresponding boundary conditions are:

$$\begin{aligned} u(x, 0) = v(x, 0) &= 0 \\ u(x, y) \rightarrow U_{\infty} \text{ as } \frac{y}{\delta(x)} &\rightarrow \infty \\ \delta \rightarrow 0 \text{ as } x &\rightarrow 0 \end{aligned} \quad (2.2.3)$$

Here the boundary-layer thickness  $\delta(x)$  is approximated based on the length of the domain  $x$  as  $\delta(x) = [\nu x / U_{\infty}]^{1/2}$ . Determining the two velocity components of (2.2.2) via

## 2.2. BOUNDARY-LAYER EQUATIONS

the derivatives of stream function  $\psi = U_\infty \delta(x) f(\eta)$ , the corresponding Blasius equation based on the similarity variable  $\eta = \frac{y}{\delta(x)} = y \sqrt{\frac{U_\infty}{\nu x}}$  can be defined by the following ordinary differential equation:

$$\frac{d^3 f}{d\eta^3} + \frac{1}{2} f \frac{d^2 f}{d\eta^2} = 0 \quad (2.2.4)$$

The boundary conditions of (2.2.4) are:

$$\begin{aligned} f = 0 \quad \text{and} \quad \frac{df}{d\eta} = 0 \quad \text{at} \quad \eta = 0 \\ \frac{df}{d\eta} \rightarrow 1 \quad \text{as} \quad \eta \rightarrow \infty \end{aligned} \quad (2.2.5)$$

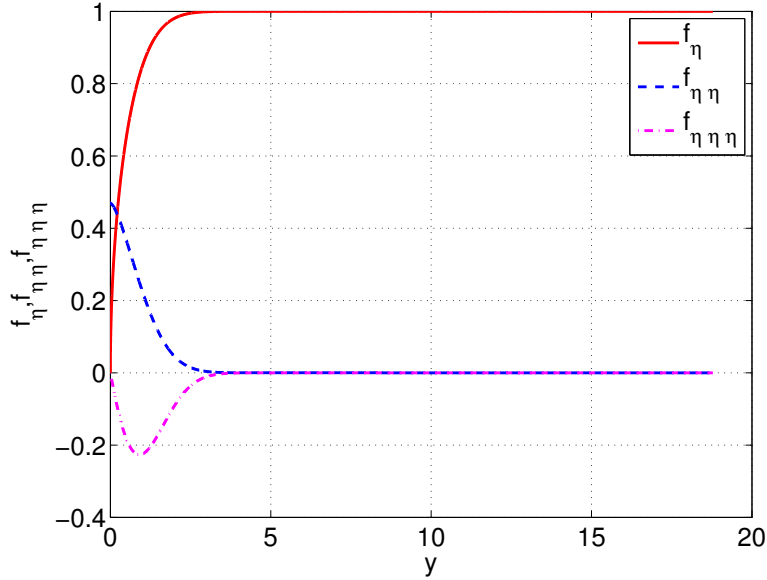


Figure 2.1: Similarity solutions of the Blasius boundary-layer equations and derivatives with respect to similarity variable  $\eta = y/\delta(x)$ .

The characteristic of the Blasius boundary-layer solutions is the slow growth rate of the boundary-layer thickness along the streamwise direction. The profile changes in a self similar way as it moves downstream. Another noteworthy property of the Blasius boundary-layer similarity profile can be achieved by the asymptotic analysis, which shows that  $(\frac{df}{d\eta} - 1) \sim \frac{1}{\eta} e^{-\frac{\eta^2}{4}}$  as  $\eta \rightarrow \infty$ . Which indicates that the streamwise velocity component  $u$  approaches free-stream velocity  $U_\infty$  very smoothly as we move further from the wall.

The solutions of (2.2.4) are known as the Blasius similarity solutions for the boundary-layer flow and are defined by two velocity components  $U_{blas}(x, y), V_{blas}(x, y)$ , with  $x$  being the streamwise direction and  $y$  normal to the wall. The similarity solutions can

be expressed in non-dimensional form as:

$$\begin{aligned} U_{blas}(y) &= \frac{u}{U_\infty} = f_\eta(\eta) \\ V_{blas}(y) &= \frac{v}{U_\infty} = \frac{1}{2Re_x^{\frac{1}{2}}}(-f(\eta) + \eta f_\eta(\eta)) \end{aligned} \tag{2.2.6}$$

According to the study of Fasel et al [6], the numerical simulation of the complete Navier-Stokes equations of a small amplitude wave showed that locally parallel theory predicts Fourier amplitude functions very well. Their results went in good agreement with the conclusion of Klingmann et al [13] justifying the use of parallel flow assumption. In this study we are also going to use parallel flow approximation which is valid for sufficiently large  $Re$ . As we see from equation (2.2.6),  $V_{blas}$  is of order  $Re_x^{-1}$ , we can assume the contribution from the wall-normal velocity component  $V_{blas}(y)$  is small enough to be negligible for large  $Re_x$ . This leads us to define the parallel laminar flow for non-thickening boundary layer as  $\mathbf{U}_{blas} \approx U_{blas}(y)\mathbf{i} = f_\eta(\eta)\mathbf{i}$ , with  $\mathbf{i}$  as a unit vector.

## Chapter 3

# Theory

Although the mathematical theory of the stability of sheared viscous flows was developed many years ago, the physical mechanism behind the process of instability has received relatively little attention, and still remains obscure. One of the common method to understand this instability in viscous boundary-layer flows is to study the Tollmein-Schlichting waves (hereafter denoted to as TS waves), which basically is the streamwise instability arises in a viscous boundary layer. This instability is the initial part of the process of transition to turbulence in boundary layers in common situations such as on aeroplane wings. In case of incompressible flow, two-dimensional TS waves are generated in the mean flow direction when some disturbance (sound for example) interacts with leading edge roughness in a process known as receptivity. These waves are slowly amplified as they move downstream until they may eventually grow large enough that nonlinearities take over and the flow transitions to turbulence. The essential mathematics of these waves originally discovered by Ludwig Prandtl, were further studied by two of his former students, Walter Tollmein and Hermann Schlichting for whom the phenomenon is named.

Transition of the laminar boundary layer to turbulence is governed by the choice of control parameter namely Reynolds number  $Re_{\delta^*}$ , based on the boundary-layer displacement thickness  $\delta^*$ . For  $Re_{\delta^*} < 17$ , the lower limit where short-lived growth of disturbance energy is possible. The laminar state is globally stable and finite-amplitude disturbances decrease monotonically [3]. Depending on the disturbance shape and energy, for the interval  $17 < Re_{\delta^*} < 519.4$  the flow is conditionally stable. On the other hand, TS traveling waves are amplified and laminar state stays no longer attractor for even weaker disturbance for  $Re_{\delta^*} > 519.4$  [3] and we can see the supercritical classical transition.

### 3.1 Forcing

When a viscous fluid flows over a solid surface in both laminar and turbulent flows, loses kinetic energy constantly because of the friction with the wall. This is happened as the molecules of the fluid right next to the surface stick to the surface. The molecules just above the surface are slowed down in their collision with the molecules sticking to the surface and these molecules in turn slow down the flow just above them. As we move away from the surface, the effect of the collision with the surface slows down. This flow deceleration near the surface in boundary-layer flows, helps growing the boundary-layer

thickness in time (Figures 3.1 and 3.2).

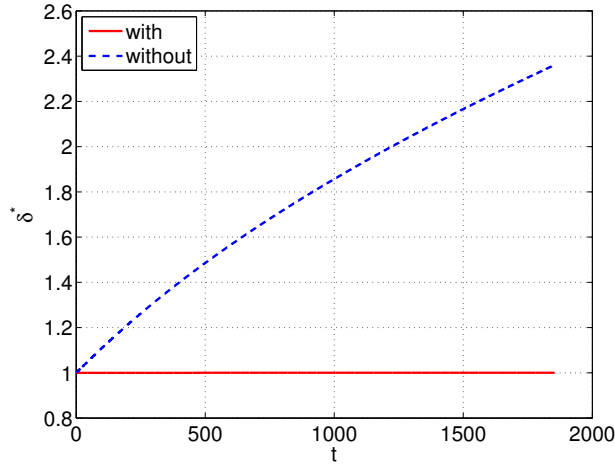


Figure 3.1: Effect of forcing in a laminar boundary-layer flow for  $Re_{\delta^*} = 510$ . Figure represents the displacement boundary layer thickness  $\delta^*$  for with and without forcing.

Widening in the boundary-layer thickness can be seen in Figure 3.1. So, to keep the flow from decelerating and to maintain a non-thickening boundary layer we need to employ proper forcing to the flow. A well-estimated forcing will ensure the correct development of the boundary layer profile. To highlight more the effect of forcing in a boundary-layer flow we present below the stream-wise velocity profile along normal direction normalized by the free stream velocity  $U_\infty$ .

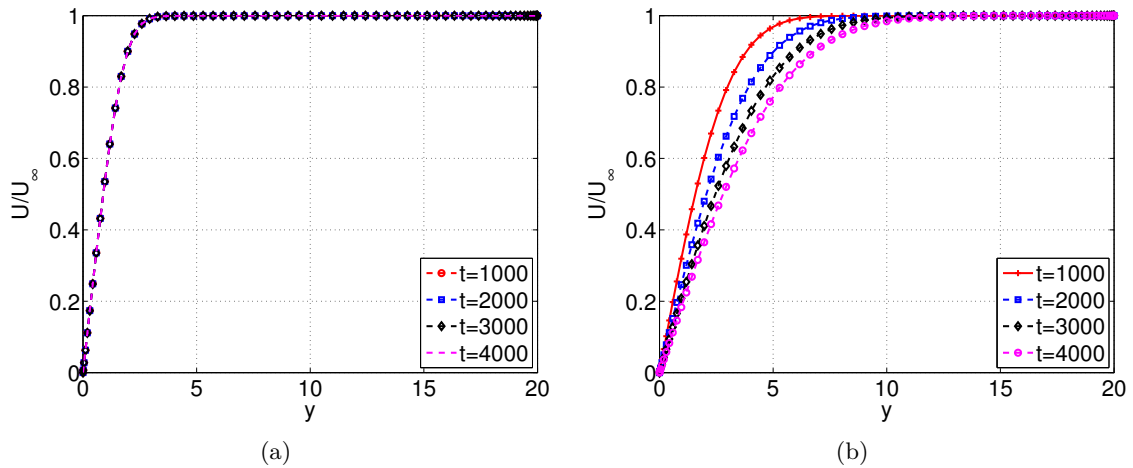


Figure 3.2: Effect of forcing in a laminar boundary-layer flow for  $Re_{\delta^*} = 510$ . (a) with force; (b) without force. Figures clearly show that the flow is slowing down near the surface as the boundary-layer thickness  $\delta_{99}$  increases in time while there is no driving force in the flow. In contrast, the velocity profiles remain almost constant in time and we don't see  $\delta_{99}$  increases for the flow with forcing. Here,  $\delta_{99}$  is an overall boundary-layer thickness that specifies the distance from the wall where the stream-wise velocity in the boundary layer is 99% of the free-stream velocity  $U_\infty$ .

### 3.1. FORCING

#### 3.1.1 Spalart and Yang method

In parallel boundary-layer flow with periodic boundary conditions in  $x$ , the mean flow is independent of streamwise direction  $x$  and the mean velocity component  $U$  is a function of the normal direction  $y$  and the time  $t$ . During the linear stage, the Reynolds stress  $\tau$  is negligible ( $\tau = -\langle u'v' \rangle$ , where  $u'$  and  $v'$  are the fluctuations along streamwise and normal directions with respect to the mean flow  $U(y, t)$ ,  $V = 0$  and  $\langle \rangle$  denotes an average over the  $x$ - and  $z$ -directions) and the mean velocity  $U$  satisfies the following equation of motion,

$$\frac{\partial U}{\partial t} = \frac{1}{Re} \frac{\partial^2 U}{\partial y^2} \quad (3.1.1)$$

where  $Re = \left(\frac{U_\infty x}{\nu}\right)^{\frac{1}{2}}$  with  $U_\infty$  as laminar free-stream velocity,  $x$  as the length of the domain and  $\nu$  as kinematic viscosity of the fluid.

Equation (3.1.1) represents the Stokes first problem, for which the solution is a thickening error function. To deal with this thickening error, Spalart and Yang [24] modified the equation (3.1.1) by adding a small correction term that should allow the thickness to grow in time instead of space, while retaining a Blasius profile. The procedure is as follows.

The boundary-layer profile is defined by the solution of the Blasius equation  $U_{blas}(y, x_r)$  as a function of  $y$  and of  $x_r$ . Here,  $x_r$  is a reference point defining the distance from the leading edge at which the mean flow is evaluated. This reference point is introduced by a linear correspondence between time  $t$  and distance  $x_r$  as follows:

$$x_r = x_0 + ct \quad (3.1.2)$$

Here  $c$  is a reference speed and is chosen to match the growth rate of the boundary-layer thickness and the growth rate of the TS wave.

Introducing the relation between  $x_r$  and  $t$  into the function  $U_{blas}(y, x_r)$  defines the desired mean velocity profile  $U_{blas}(y, t)$ . The correction to the  $U$ -component momentum equation consists of the quantity  $\frac{\partial U_{blas}}{\partial t} - \frac{1}{Re} \frac{\partial^2 U_{blas}}{\partial y^2}$ , which depends only on  $y$  and  $t$ . Thus the modified equation of motion (3.1.1) becomes

$$\frac{\partial U}{\partial t} = \frac{1}{Re} \frac{\partial^2 U}{\partial y^2} + \frac{\partial U_{blas}}{\partial t} - \frac{1}{Re} \frac{\partial^2 U_{blas}}{\partial y^2} \quad (3.1.3)$$

Now, if the initial profile is the Blasius solution

$$U(y, 0) = U_{blas}(y, 0) \quad (3.1.4)$$

the solution  $U(y, t)$  of (3.1.3) and (3.1.4) will satisfy

$$U(y, t) = U_{blas}(y, t) \quad (3.1.5)$$

Thus the correction term to the streamwise momentum equation can be viewed as forcing as follows:

$$\begin{aligned} F_1 &= \frac{\partial U_{blas}(y, t)}{\partial t} - \frac{1}{Re} \frac{\partial^2 U_{blas}(y, t)}{\partial y^2} \\ &= c \frac{\partial U_{blas}(x, y)}{\partial x} - \frac{1}{Re} \frac{\partial^2 U_{blas}(x, y)}{\partial y^2} \end{aligned} \quad (3.1.6)$$

Equation (3.1.6) shows that if the reference speed  $c$  is zero, the forcing term reduces to

$$F_1 = -\frac{1}{Re} \frac{\partial^2 U_{blas}(y, t)}{\partial y^2}$$

### 3.1.2 Wedin *et al* study

In their study, Wedin *et al* [9] used the forcing term  $F_1 = -\frac{1}{Re} \frac{\partial^2 U_{blas}(y, t)}{\partial y^2}$  to the stream-wise momentum equation to account for the parallel base flow. Their study was similar to Rotenberry (1993) [26] and Milinazzo & Saffman (1985) [19]. Wedin *et al* [9] adapted the forcing term along with the magnitude for the perturbation equations.

Following the idea of Koch [14], the instantaneous velocity field  $\mathbf{u}$  is decomposed as a local boundary layer profile  $\mathbf{U}_{base} = (U_{base}, V_{base}, W_{base})$  plus the disturbances  $\mathbf{u}' = (u', v', w')$ . Thus the total velocity field can be defined as follows:

$$\mathbf{u} = \mathbf{U}_{base} + \mathbf{u}'$$

To define the base flow, parallel flow assumption for the two-dimensional laminar Blasius solution was used described in previous Chapter as  $\mathbf{U}_{base} = U_{blas}(y)\mathbf{i} = f_\eta(\eta)\mathbf{i}$ . Which means that the normal and spanwise components of base flow are both zero and we only have non-zero streamwise component of base flow  $U_{base}$ . i.e  $V_{base} = W_{base} = 0$  and  $U_{base} = U_{blas}(y)$ .

Since  $U_{blas}$  is a function of  $y$  only, consequently the base flow  $\mathbf{U}_{base}$  is a function of  $y$  only, meaning we are assuming the flow through a parallel boundary layer. This helps us to assume that the solution is periodic. We also assume the disturbance  $\mathbf{u}'$  to be separable in  $x, z$  and  $t$ . Thus we can express the streamwise and spanwise dependence of each variable as:

$$\begin{aligned} \mathbf{u}(x, z) &= U_{base}(y)\mathbf{i} + \mathbf{u}' \\ \Rightarrow \sum_{l=-\frac{N_x}{2}-1}^{\frac{N_x}{2}-1} \sum_{m=-\frac{N_z}{2}-1}^{\frac{N_z}{2}-1} \hat{\mathbf{u}}_{tot}^{lm} e^{i(\alpha_l x + \beta_m z)} &= U_{base}(y)\mathbf{i} + \sum_{l=-\frac{N_x}{2}-1}^{\frac{N_x}{2}-1} \sum_{m=-\frac{N_z}{2}-1}^{\frac{N_z}{2}-1} \tilde{\mathbf{u}}_{pert}^{lm} e^{i(\alpha_l x + \beta_m z)} \end{aligned} \quad (3.1.7)$$

where  $N_x$  and  $N_z$  are the number of Fourier modes in the streamwise and spanwise direction respectively,  $\alpha_l$  and  $\beta_m$  are real wave numbers defined as  $\alpha_l = 2\pi l/x_l$  and  $\beta_m = 2\pi m/z_l$ , imaginary variable  $i = \sqrt{-1}$ ,  $\hat{\mathbf{u}}_{tot}^{lm}(y)$  represents the Fourier mode for the total flow and  $\tilde{\mathbf{u}}_{pert}^{lm}(y)$  denotes Fourier mode for the disturbances.

Asymptotically decaying boundary condition ( $(\tilde{\mathbf{u}}_{pert}^{lm})_y + (l^2 \alpha_l^2 + m^2 \beta_m^2) \tilde{\mathbf{u}}_{pert}^{lm} = 0$ ) was imposed in their study to make sure that the Fourier mode  $\tilde{\mathbf{u}}_{pert}^{00}(y)$  for the perturbation decays to zero to account for the parallel base flow at  $y = y_{max}$ . But the  $\tilde{u}_{pert}^{00}(y)$  mode does not decay exponentially to zero for  $y = y_{max}$  and is thus finite with zero gradient at  $y = y_{max}$ , which means the flow at the outer edge of the domain fails to stay unperturbed. So, to ensure unperturbed flow at  $y = y_{max}$  the base flow  $U_{base}$  needs to act as a corrector on the assumption of uniform flow  $\mathbf{u} = (1, 0, 0)$  at the free-stream. Therefore the base flow is set equal to

$$U_{base}(y) = U_{blas}(y) = K_p f_\eta(\eta) \quad (3.1.8)$$

### 3.1. FORCING

The coefficient  $K_p$  serves to ensure that the correct asymptotic boundary condition is satisfied. Relevant studies were performed by Milinazzo & Saffman (1985) [19]; Koch (1992) [14]; Rotenberry(1993) [26] and Ehrenstein & Rossi (1996) [5] to maintain the uniform flow at the outer edge of the domain in the presence of finite amplitude perturbations. Thus the condition to fulfill the uniform flow at the free-stream is:

$$\begin{aligned} K_p f_\eta(y_{max}) + \tilde{u}_{pert}^{00}(y_{max}) &= 1 \\ \Rightarrow K_p + \tilde{u}_{pert}^{00}(y_{max}) &= 1 \end{aligned} \quad (3.1.9)$$

Equations (3.1.8) and (3.1.9) show that  $K_p = 1$  for purely laminar flow and infinitesimal disturbances, while in the presence of finite amplitude disturbances  $K_p$  is different from unity.

#### 3.1.3 Present study

The present study is based on the studies performed by Wedin *et al* [9] and Spalart and Yang (1985) [24]. The forcing term ( $F_1 = -\frac{1}{Re} \frac{\partial^2 U_{blas}(y,t)}{\partial y^2} = -\frac{1}{Re} \frac{\partial^2 (K_p f_\eta(\eta))}{\partial y^2}$ ) added to the streamwise momentum equation is same as Spalart and Yang (1985) [24] in the absence of reference speed  $c$  along with the magnitude coefficient  $K_p$ . To adjust the magnitude of the forcing term, we borrowed the idea from Wedin *et al* [9] and introduced the adapted forcing term to the total flow fields rather than the perturbation equations.

Combining the equations (3.1.7) and (3.1.9) we got the following relation for  $K_p$  and total Fourier mode  $u_{tot}^{00}(y_{max})$ :

$$\begin{aligned} K_p + u_{tot}^{00}(y_{max}) - U_{base}(y_{max}) &= 1 \\ \Rightarrow K_p &= 1 + U_{base}(y_{max}) - u_{tot}^{00}(y_{max}) \end{aligned} \quad (3.1.10)$$

Equation (3.1.10) leaves us with two choices based on  $U_{base}(y_{max})$ .

#### Non-iterative approach

$U_{base}(y_{max})$  could be set as the value of the initial base flow at  $y_{max}$  to compute  $K_p$ ; i.e.  $U_{base}(y_{max}) = f_\eta(y_{max}) = 1$  at every step. In this case, we have the forcing magnitude  $K_p = 2 - u_{tot}^{00}(y_{max})$ .

#### Iterative approach

At each time step  $U_{base}(y_{max})$  can be computed based on the base flow calculated on the previous step ( $U_{base}(y_{max}) = K_p f_\eta(y_{max}) = K_p$ ). In the presence of finite amplitude disturbances  $K_p$  value would be different from unity, which mean  $U_{base}(y_{max})$  will also be changed as  $K_p$  changes. This updated  $U_{base}(y_{max})$ , which is nothing but the  $K_p$  value of the previous step, could be used to compute  $K_p$  for the current step iteratively.

In this study we are going to use the first option, that is the non-iterative approach. We leave the iterative approach for the future study.

### 3.1.4 Forcing profile

We have seen that the forcing term got the expression  $-\frac{1}{Re} \frac{\partial^2 (K_P f_\eta(\eta))}{\partial y^2}$ . This indicates that the forcing is proportional to the negative of  $f_{\eta\eta\eta}$ , which is the third derivative of the Blasius similarity solution of the boundary layer equation 2.2.4, where the derivative is with respect to the similarity variable  $\eta$ .

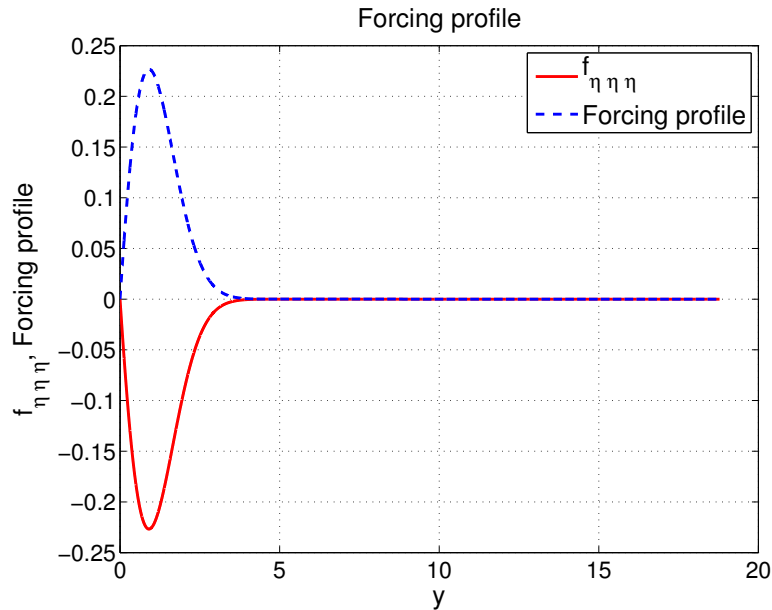


Figure 3.3: Forcing profile is proportional to  $-f_{\eta\eta\eta}$  for amplitude  $K_P = 1$ .

From the above figure we see that the forcing is applied up to the initial boundary layer thickness  $\delta_{99}$  and above that the profile becomes zero. Here,  $\delta_{99}$  is an overall boundary-layer thickness that specifies the distance from the wall where the stream-wise velocity in the boundary layer is 99% of the free-stream velocity  $U_\infty$ .

## 3.2 Boundary conditions

Boundary conditions in the horizontal directions are periodic. However, we need to specify boundary conditions at the wall and in the free-stream. Various boundary conditions can be tested along the wall-normal direction. At the wall we impose vanishing (no-slip) boundary condition. But to specify the boundary conditions in the free-stream we can choose one of the boundary conditions describe below.

Despite the flow is assumed to extend infinitely far perpendicular to the wall, for practical reason we have to truncate the domain to a finite distance. Say, the outer edge of the domain locate at a wall-normal position  $y_{max}$  and we need to apply an artificial boundary condition at this point. The simplest choice could be the Dirichlet boundary condition defined as:

$$\mathbf{u}|_{y=y_{max}} = \mathbf{U}_{base}|_{y=y_{max}} \quad (3.2.1)$$

### 3.2. BOUNDARY CONDITIONS

where  $\mathbf{U}_{base}(y)$  is the similarity solution to the Blasius boundary-layer equations.

Generally we are interested in a flow that will contain a disturbance. But forcing this disturbance to be zero at the free-stream by imposing Dirichlet condition, results in an error to the exact solution for which the boundary condition is applied at an infinite distance from the wall. The error may over-damp the disturbances in the boundary layer. This error can be minimized by choosing the Neumann condition defined as:

$$\frac{\partial \mathbf{u}}{\partial y} \Big|_{y=y_{max}} = \frac{\partial \mathbf{U}_{base}}{\partial y} \Big|_{y=y_{max}} \quad (3.2.2)$$

But most appropriate boundary condition could be to use the generalization of the boundary condition proposed by Malik *et al* (1985) [17], which allows the boundary to be placed closer to the wall. This asymptotic boundary condition can be easily applied in Fourier space that decreases the error further and is defined in terms of horizontal Fourier transform with respect to the horizontal coordinates as:

$$\left( \frac{\partial \hat{\mathbf{u}}}{\partial y} + |k| \hat{\mathbf{u}} \right) \Big|_{y=y_{max}} = \left( \frac{\partial \hat{\mathbf{U}}_{base}}{\partial y} + |k| \hat{\mathbf{U}}_{base} \right) \Big|_{y=y_{max}} \quad (3.2.3)$$

where  $\hat{(\cdot)}$  denotes the horizontal Fourier mode in the horizontal directions and  $k^2 = \alpha^2 + \beta^2$  with  $\alpha$  and  $\beta$  are the horizontal wavenumbers (see equation (3.1.7)). This boundary condition ensures that the potential flow solution decays away from the wall.

In the present study we have chosen the boundary condition defined in 3.2.3.



## Chapter 4

# Numerical Method

For numerical simulations, the unsteady incompressible Navier-Stokes equations were solved within a numerical domain defined as  $[-L_x/2, L_x/2] \times [0, L_y] \times [-L_z/2, L_z/2]$ .

An equation for the normal velocity component can be found by taking the divergence of the momentum equations of (2.1.3) updated by adding the forcing term to the right hand side. For numerical purposes, they can be written as a system of two second order equations

$$\frac{\partial \psi}{\partial t} = G + L\psi \quad (4.0.1)$$

with  $\psi = \nabla^2 v$ . Here, operator  $G$  contains the non-linear advective and forcing terms and depends on all velocities and vorticities.  $L$  represents the linear diffusion term. A similar form as (4.0.1) can be found for the normal vorticity  $\omega$  by taking the curl of the updated momentum equations of (2.1.3). Once the normal velocity  $v$  and the normal vorticity  $\omega$  have been calculated the other velocity components can be found from the incompressibility constraint and the definition of the normal vorticity.

### 4.1 Temporal discretization

The time advancement is carried out by one out of two semi-implicit schemes. Operator  $G$  is discretized explicitly by a low storage third order three or four stage Runge-Kutta(RK3) scheme, while the linear diffusion term  $L$  is discretized implicitly using the second order accurate Crank-Nicolson(CN) scheme. These time discretization may be written in the following manner

$$\psi^{n+1} = \psi^n + a_n G^n + b_n G^{n-1} + (a_n + b_n) \left( \frac{L\psi^{n+1} + L\psi^n}{2} \right) \quad (4.1.1)$$

Here,  $a_n$  and  $b_n$  are time stepping coefficients, which are chosen according to the explicit scheme used and  $G$  and  $L$  are assumed to have no explicit dependence on time. One full physical time step is only achieved every three or four iterations based on Runge-Kutta scheme.  $t = t + c_n$  defines the time used for the intermediate stages. The two possibilities for the  $RK3$  schemes are shown in the table below.

	$a_n/\Delta t^n$	$b_n/\Delta t^n$	$c_n/\Delta t^n$
RK3 3-stage	8/15	0	0
	5/12	-17/60	8/15
	3/4	-5/12	2/3
RK3 4-stage	8/17	0	0
	17/60	-15/68	8/17
	5/12	-17/60	8/15
	3/4	-5/12	2/3

Table 4.1: Time stepping coefficients. Table source [18].

## 4.2 Space discretization: Horizontal direction

Fourier series expansion is used to discretize in the horizontal directions which assumes that the solution is periodic. The streamwise and spanwise dependence of each variable can be written similar to equation (3.1.7) for the Fourier modes  $N_x$  and  $N_y$  along streamwise and spanwise directions

$$u(x, z) = \sum_{l=-(\frac{N_x}{2}-1)}^{\frac{N_x}{2}-1} \sum_{m=-(\frac{N_z}{2}-1)}^{\frac{N_z}{2}-1} \hat{u}^{lm}(\alpha_l, \beta_m) e^{i(\alpha_l x + \beta_m z)} \quad (4.2.1)$$

Here,  $\alpha_l$  and  $\beta_m$  are real wave numbers defined as  $\alpha_l = 2\pi l/x_l$  and  $\beta_m = 2\pi m/z_l$ .

## 4.3 Space discretization: Normal direction

To discretize in the normal direction for boundary-layer flow, first it requires to map the physical domain  $[0, y_{max}]$  to  $[-1, 1]$  by setting  $y' = 2y/y_{max} - 1$ . Then the dependent variable  $\hat{\psi}$  is expanded in Chebyshev series, *i.e.*,

$$\hat{\psi}(y) = \sum_{j=0}^{N_y} \tilde{\psi}_j T_j(y) \quad (4.3.1)$$

where  $T_j$  are the Chebyshev polynomial of order  $j$  and  $N_y$  the highest order of polynomial included in the expansion. For simplicity we dropped the prime of  $y$  in the above equations.

For more details on numerical implementation, please refer to [18].

## 4.4 Properties of the discretizations

To analyse some properties of the discretizations they will be applied to the two dimensional linearized Burgers' equation with a system rotation. The eigenvalue analysis yields a necessary condition for stability. Putting the equation into the form of equation

#### 4.4. PROPERTIES OF THE DISCRETIZATIONS

(4.0.1) yields

$$\begin{aligned}
 \psi &= \begin{bmatrix} u \\ w \end{bmatrix} \\
 G &= \begin{bmatrix} u_0 \frac{\partial}{\partial x} + w_0 \frac{\partial}{\partial z} & 2\Omega \\ -2\Omega & u_0 \frac{\partial}{\partial x} + w_0 \frac{\partial}{\partial z} \end{bmatrix} \begin{bmatrix} u \\ w \end{bmatrix} \\
 L &= \frac{1}{Re} \begin{bmatrix} \frac{\partial^2}{\partial x^2} + \frac{\partial^2}{\partial z^2} & 0 \\ 0 & \frac{\partial^2}{\partial x^2} + \frac{\partial^2}{\partial z^2} \end{bmatrix}
 \end{aligned} \tag{4.4.1}$$

where  $u_0$  and  $w_0$  represent the flow field around which the linearization was made and  $\Omega$  represents the angular velocity of the coordinate frame. The dependence of  $\psi$  on both the streamwise and spanwise coordinate directions have been included in order to indicate how multiple dimensions enter into the stability considerations.

For simplicity, Fourier discretization has been used here in the spatial directions. The Chebyshev method acts locally as a transformed Fourier method and thus the stability properties derived here can be applied with the local space step. For more details please refer to [18].

Fourier transforming in  $x$ - and  $z$ -directions yields

$$\hat{\psi}_t = \begin{bmatrix} i\alpha u_0 + i\beta w_0 & 2\Omega \\ -2\Omega & i\alpha u_0 + i\beta w_0 \end{bmatrix} \hat{\psi} - \frac{\alpha^2 + \beta^2}{Re} \hat{\psi} \tag{4.4.2}$$

where  $\alpha$  and  $\beta$  are the real wavenumbers in the  $x$ - and  $z$ -directions, respectively. The diagonalized form of this equation give the following equation,

$$\hat{u}_t = i(\alpha u_0 + \beta w_0 \pm 2\Omega) \hat{u} + \frac{\alpha^2 + \beta^2}{Re} \hat{u} \tag{4.4.3}$$

If  $\Delta x$  and  $\Delta z$  are the discretization step lengths in physical space, we assume that the stability limit will first be reached for the largest wavenumbers of the discretization  $\alpha_{max}$  and  $\beta_{max}$ , which corresponds to a wavelength of  $2\Delta x$  and  $2\Delta z$ , respectively. The important parameters for analysis are as follows,

$$\begin{aligned}
 \mu &= \Delta t(2|\Omega| + (\alpha_{max}|u_0| + \beta_{max}|w_0|)) \\
 &= \Delta t(2|\Omega| + \pi(\frac{|u_0|}{\Delta x} + \frac{|w_0|}{\Delta z}))
 \end{aligned} \tag{4.4.4}$$

$$\begin{aligned}
 \lambda &= \frac{1}{Re} \Delta t(\alpha_{max}^2 + \beta_{max}^2) \\
 &= \frac{1}{Re} \pi^2 \Delta t(\frac{1}{\Delta x^2} + \frac{1}{\Delta z^2})
 \end{aligned} \tag{4.4.5}$$

The parameter  $\mu$  is usually called the spectral CFL number, in analogy with the stability theory for finite difference equations. We have the following three stages in each time step for the modal equations (4.4.3) using the RK3-CN time discretization,

$$\begin{aligned}
 \hat{u}^{n+1} &= \hat{u}^n + i\mu a_1 \hat{u}^n - \frac{\lambda}{2} a_1 (\hat{u}^{n+1} + \hat{u}^n) \\
 \hat{u}^{n+2} &= \hat{u}^{n+1} + i\mu(a_2 \hat{u}^{n+1} + b_2 \hat{u}^n) - \frac{\lambda}{2} (a_2 + b_2) (\hat{u}^{n+2} + \hat{u}^{n+1}) \\
 \hat{u}^{n+3} &= \hat{u}^{n+2} + i\mu(a_3 \hat{u}^{n+2} + b_3 \hat{u}^{n+1}) - \frac{\lambda}{2} (a_3 + b_3) (\hat{u}^{n+3} + \hat{u}^{n+2})
 \end{aligned} \tag{4.4.6}$$

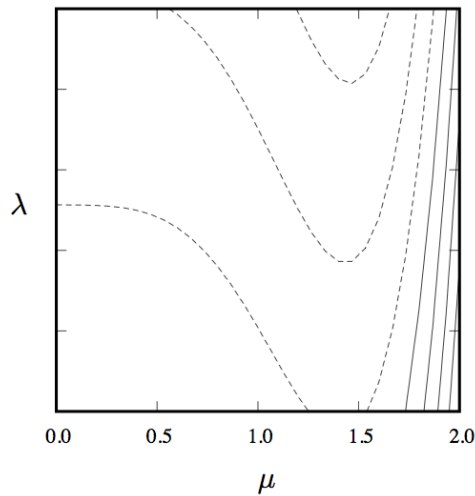


Figure 4.1: Contours of constant amplification factor for the RK3-CN method. Contour spacing is 0.05 with dashed lines indicating that the amplification factor is below unity. Figure source [18].

The regions where all solutions to the above difference equations are bounded in the  $\mu - \lambda$  plane, can now be found by calculating the roots of the associated characteristic polynomials. Contours of constant absolute values of the roots, for the RK3-CN method, are given in the Figure 4.1. Note that the method is stable for higher values of  $\lambda$  (lower  $Re$ ), *i.e.* increases the CFL number  $\mu$  that is allowed for an absolutely stable solution. In the limit of infinite Reynolds number the RK3-CN method approaches the limit  $\sqrt{3}$ . The analysis for the four stage method is analogous and the stability limit is  $\sqrt{8}$ . Reference [18].

## 4.5 Edge tracking

The dynamics on the invariant phase-space region separating trajectories that relaminarize from those experiencing turbulent dynamics, *i.e.* the separatrix was tracked using the bisection technique described by Skufca *et al* [30]. The algorithm starts with choosing two bracketing initial conditions, one leading to turbulence ( $\mathbf{u}_T$ ) and the other going laminar ( $\mathbf{u}_L$ ) as they are evolved in time. The algorithm is initialized with a turbulent flow but the choice of initial state is not critical since arbitrary initial conditions appear to converge to the same solution. Now, as the edge of chaos lies somewhere in-between, we perform a bisection on the line connecting the two. A set of initial conditions based on the weighted disturbances is considered as follows:

$$\mathbf{u}_\lambda = \mathbf{u} + \lambda(\mathbf{u}_T - \mathbf{u}_L) \quad (4.5.1)$$

where  $\lambda$  is the bisection parameter varied between 0 and 1. Initial conditions corresponding to various values of  $\lambda$  are evolved in time until they approach either the laminar or the turbulent state, according to the predefined thresholds for the root-mean-square(r.m.s) value of the wall-normal velocity fluctuations  $v_{rms}$ . Depending on which side the trajectory ends, a new initial condition is chosen by rescaling  $\lambda$  and the process is repeated. By increasing  $\lambda$ , the initial condition moves away from the laminar profile and will not become laminar again. On the other hand, to move the initial condition closer to the

#### 4.5. EDGE TRACKING

laminar profile  $\lambda$  is reduced so that the flow will not become turbulent again. Therefore by iteratively bisecting the value of  $\lambda$ , an interval of  $\lambda$  can be found bounded by a trajectory becoming turbulent at one end and the other end is bounded by a trajectory that returns to the laminar state. That is, we bracket the laminar-turbulent boundary and obtain a trajectory that evolves for a substantial long interval on the separatrix without becoming either laminar or turbulent. Thus the numerical method is based on a bisection algorithm in order to find the amplitude of two initial conditions on either side of the edge state. But because of the exponential separation of initially nearby trajectories and the limited numerical accuracy of the bisection, the two states quickly separates in the edge's unstable direction and the resulting trajectory visits the boundary for a finite time only. That is why, a refining bisection is required to find a new pair of states that are close together. This can be done by restarting the bisection (after every 1500 time units in our case) from the last state closest to the edge often enough to constrain the solution on the separatrix that shadows the basin boundary for an infinite time to reach a relative attractor within this boundary, the edge state. The main steps of the algorithm are shown in the following Figure 4.2.

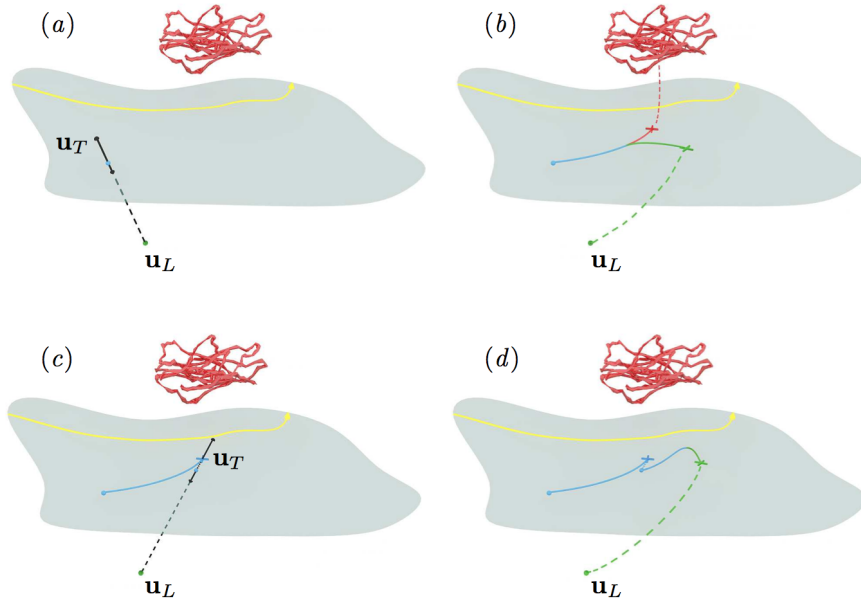


Figure 4.2: Conceptual sketch of the phase space illustrating edge-tracking algorithm. Green dot represents the laminar state and the convoluted red structure represents the turbulence. Laminar-turbulent boundary is illustrated by the grey surface, with the edge state representing by the yellow curve. (a) The family of initial conditions used for the bisection is represented by a part (solid) of the black dashed line connecting two states from both sides of the boundary,  $\mathbf{u}_T$  and  $\mathbf{u}_L$ ; (b) Two trajectories shadowing the separatrix obtained with the bisection and later leave it in two different directions; (c) The last trajectory of the current bisection and the family of initial conditions for the next one and (d) Results of the following bisection. Figure source [33] with kind permission.



## Chapter 5

# Validation and results

This chapter is dedicated to the validation and the comparison of our results with the Spalart and Yang method [24]. The results were collected using the open source code SIMSON [18], where Spalart and Yang method has already been implemented. To get the results for the present method, we have adapted the amplitude of the forcing term used in Spalart and Yang method in the SIMSON code [18]. We have implemented our adaptive forcing amplitude technique for three different cases categorized as 2D, 3D and the edge state. For 2D case, a two-dimensional domain with periods  $L_x = 20$  and  $L_y = 20$ , normalized by the displacement thickness  $\delta^*$  was chosen. On the other hand, the periods for 3D case are  $L_x = 20$ ,  $L_y = 20$  and  $L_z = 6$  and for the edge state are  $L_x = 10$ ,  $L_y = 20$  and  $L_z = 6$ .

The Reynolds number was decided based on the critical value 519.4. At least one sub-critical and one super-critical Reynolds number were chosen for 2D and 3D cases. For the edge tracking a sub-critical Reynolds number was considered.

### 5.1 2D

In 2D case our main aim is to check whether our method works by comparing and validating our results with the Spalart and Yang method. The comparison and validation have been done for the Reynolds number  $Re_{\delta^*} = 510$  and  $Re_{\delta^*} = 600$ . To analyze 2D case further for our method we chose another super-critical Reynolds number  $Re_{\delta^*} = 1000$ . In all simulations for 2D case the number of spectral nodes in  $x$  and  $y$  directions is  $(64 \times 65)$ .

Introduction of localized disturbance with reasonably small amplitude to the initial Blasius profile for both sub-critical and super-critical Reynolds number has been studied for present method along with Spalart and Yang method. We performed all simulations with Blasius profile disturbed by localized disturbance as initial condition. Studies have shown that for sub-critical Reynolds number, the disturbance energy decreases exponentially in time and eventually everything will be damped out to zero to restore the initial Blasius laminar profile. On the other hand, for super-critical Reynolds number the boundary-layer flow develops TS waves with growing amplitude and saturation. Figure 5.1(a) shows the exponential decay of the TS waves energy and free-stream recovering the uniform flow condition as  $u_{tot}^{00}(y_{max})$  mode (Figure 5.1(b)) converging to 1. Displacement thickness (Figure 5.1(c)) and  $\delta_{99}$  (Figure 5.1(d)) also converging to the laminar value in the advancement of time. These clearly indicate that the solution retains to the

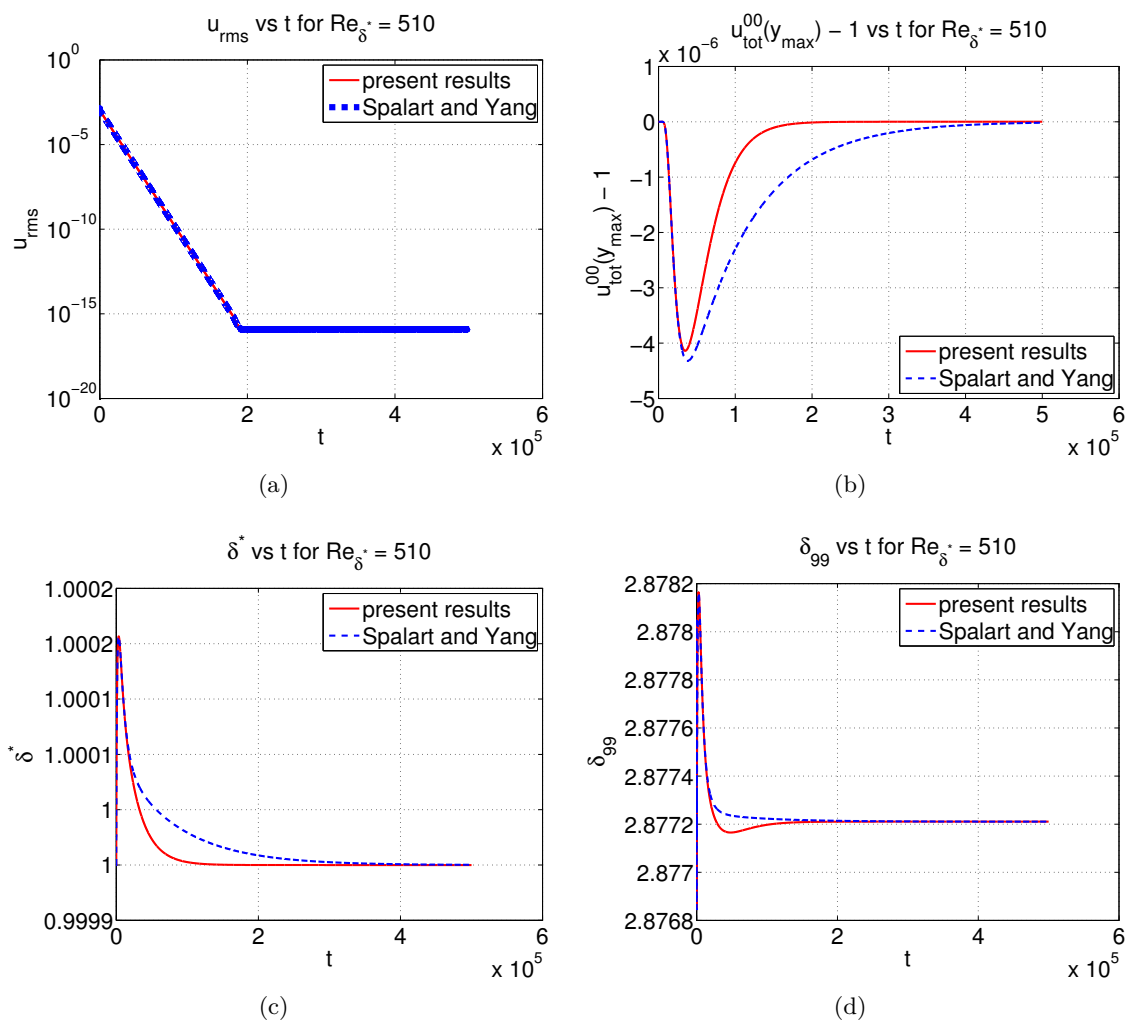


Figure 5.1: Validating results with Spalart and Yang method for  $Re_{\delta^*} = 510$ . Figures show the time evolution of (a) energy of TS waves  $u_{rms}$ ; (b)  $u_{tot}^{00}(y_{max}) - 1$ ; (c) displacement thickness  $\delta^*$  and (d)  $\delta_{99}$ .

laminar Balsius profile both for the present method and the Spalart and Yang method for sub-critical Reynolds number  $Re_{\delta^*} = 510$ .

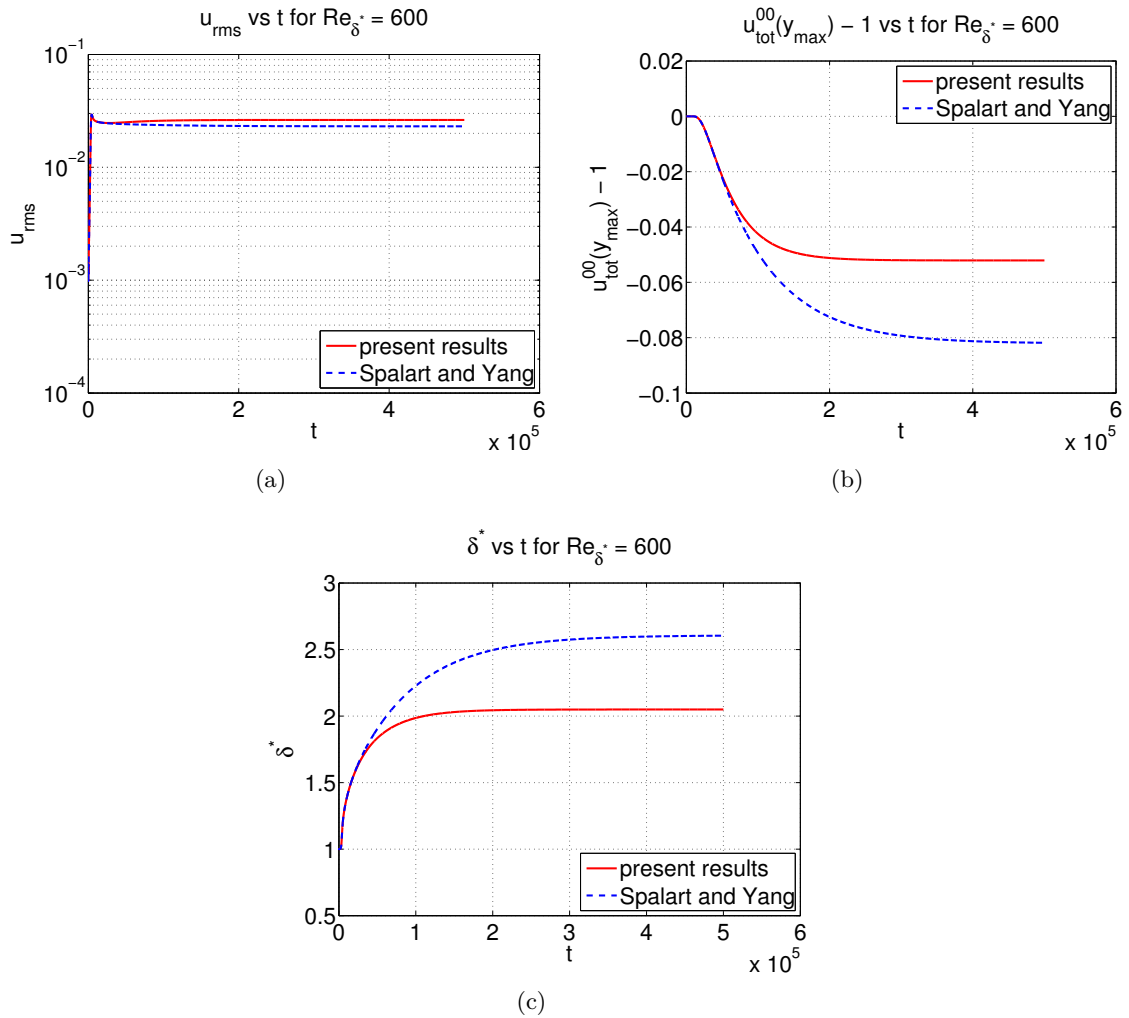


Figure 5.2: Comparing results with Spalart and Yang method for  $Re_{\delta^*} = 600$ . To calculate  $\delta^*$  and  $\delta_{99}$  initial free-stream value  $U_\infty = 1$  was assumed. Figures show the time evolution of (a) energy of TS waves  $u_{rms}$ ; (b)  $u_{tot}^{00}(y_{max}) - 1$  and (c) displacement thickness  $\delta^*$ .

For super critical Reynolds number  $Re_{\delta^*} = 600$ , using the same initial condition as  $Re_{\delta^*} = 510$ , the disturbance energy increases as expected. In both present and Spalart and Yang method we see that the disturbance amplitude increases in time and after certain time the disturbance becomes almost steady (Figure 5.2(a)). This energy increasing in disturbance slows down the flow and results in the growth of displacement thickness (Figure 5.2(c)). As the disturbance never vanishes, rather it is in the flow, the finite amplitude disturbance dominates the forcing term and never let free-stream to retain initial laminar state (Figure 5.3(b)).

Both the present and Spalart and Yang method exhibit the similar flow pattern, the solutions are not exactly identical, at least in case of super-critical Reynolds number. We can see that the mean velocity at the at the free-stream defined by  $u_{tot}^{00}(y_{max})$  mode (Figure 5.2(b)) is decreasing because of disturbance in the flow. The forcing amplitude for the present method by definition is increasing, while for Spalart and Yang method it is constant. The effects of this difference in the forcing amplitude for both methods is clearly distinguishable in Figures 5.2(a), 5.2(b), 5.2(c) and 5.3(b). In Figure 5.3(b) we can see that the free-stream is perturbed by the disturbance and the value goes below 1 for both methods. Though the velocity profiles are similar for both methods, they slightly lose the Blasius shape and the correction term becomes inadequate to retain the initial laminar state. The only difference between the methods is that the present method maintains slightly larger value for  $u/U_{\infty}$  away from the wall compare to the Spalart and Yang. On the contrary, for sub-critical Reynolds number, both methods converge to the initial Blasius profile (Figure 5.3(a)).

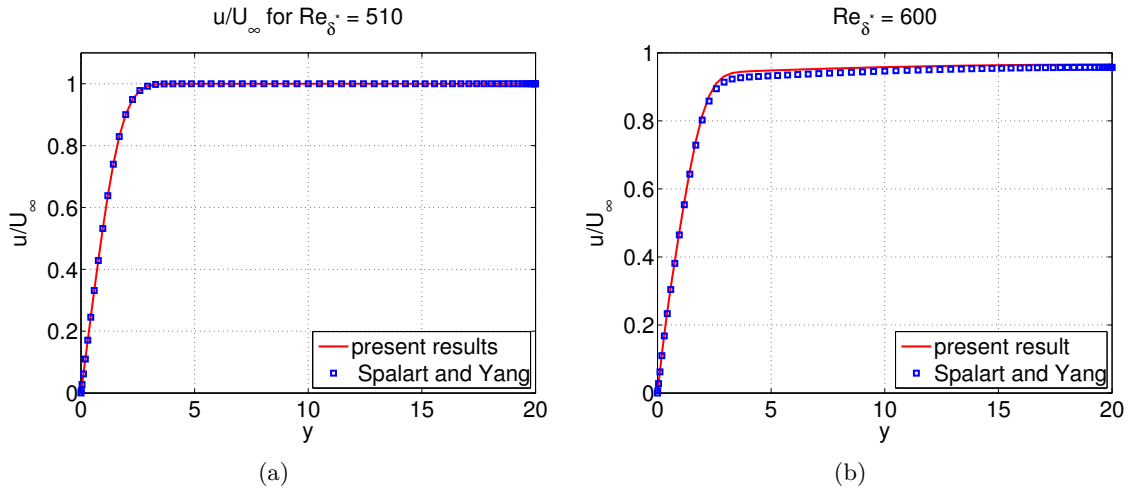


Figure 5.3: Mean velocity profile non-dimensionalized by the free-stream velocity  $U_{\infty}$  at  $x = 0$ . a)  $Re_{\delta^*} = 510$ ; b)  $Re_{\delta^*} = 600$ .

5.1. 2D

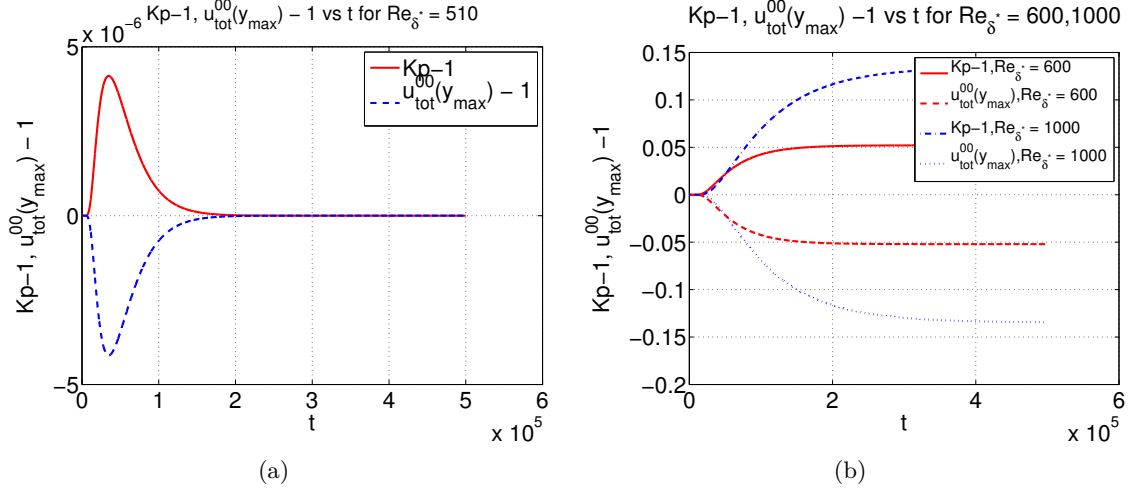


Figure 5.4: Time evolution of the forcing amplitude  $K_p$  and the  $u_{tot}^{00}(y_{max})$  mode for the present method. a) Converging characteristic for  $Re_{\delta^*} = 510$ ; b) Steady state for  $Re_{\delta^*} = 600, 1000$ .

Figure in 5.4(a) represents the converging criteria of the  $u_{tot}^{00}(y_{max})$  mode and the forcing amplitude  $K_p$  for sub-critical Reynolds number to the laminar value  $u_{tot}^{00}(y_{max}) = 1$  and  $K_p = 1$ . But for the super-critical Reynolds number mean velocity at the edge of the domain  $u_{tot}^{00}(y_{max})$  decreases in time, consequently the forcing amplitude  $K_p$  increases (Figure 5.4(b)). After certain instant of time unit the flow seems to become steady and mean velocity turns to be constant, so does  $K_p$ . This also indicates that the flow is never restored to the laminar Blasius flow rather it conceives the disturbance in it. We could see the wave-like disturbance, so called TS waves, moving with the flow with saturated disturbance and increase in energy in the advancement of time in the Figures 5.5 and 5.6 for  $Re_{\delta^*} = 600$  for both the present method and Spalart and Yang method.

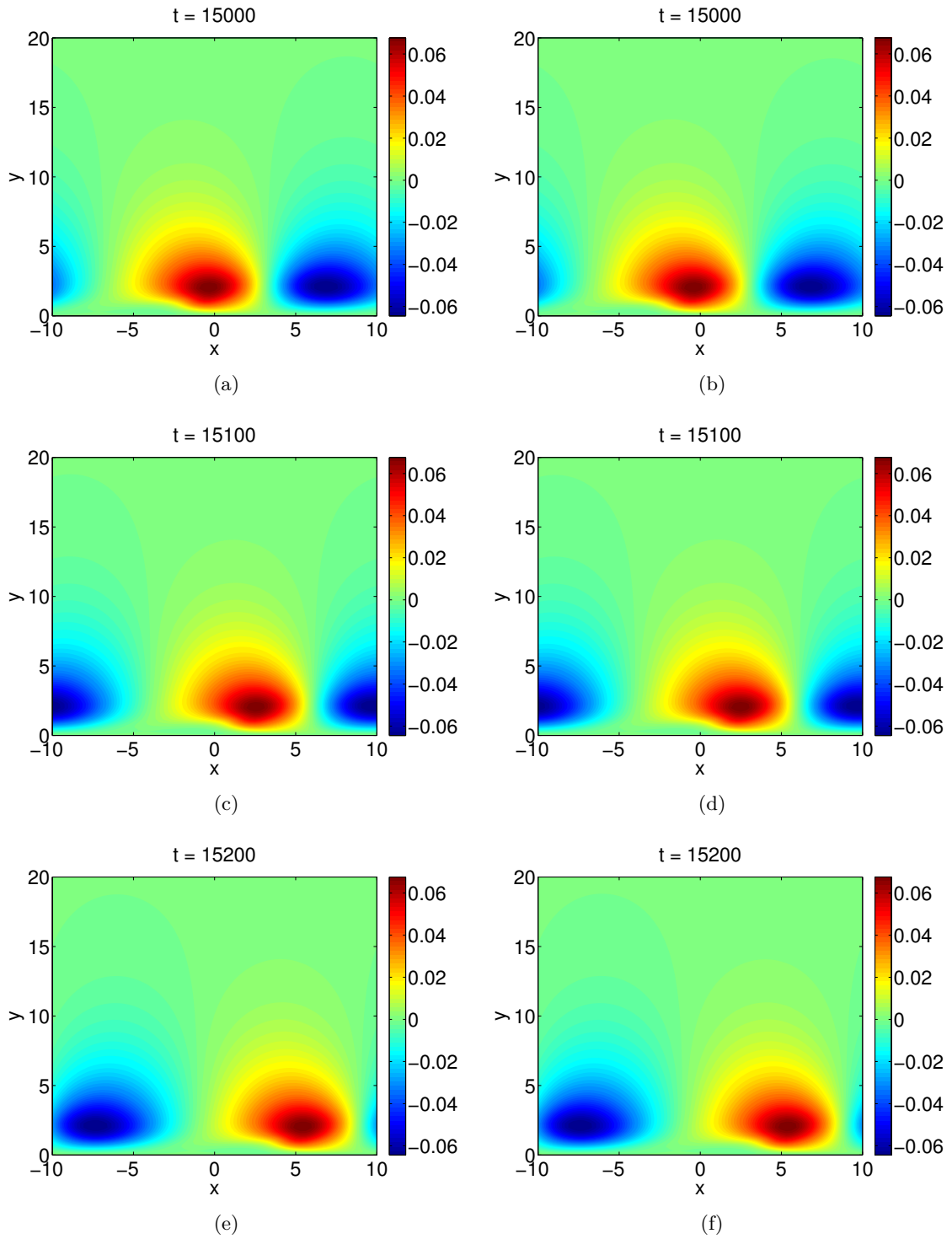


Figure 5.5: Visualization of the travelling of TS waves along streamwise direction at time  $t = 15000, 15100$  and  $15200$  for  $Re_{\delta^*} = 600$ . (a), (c), (e) Present results; (b), (d), (f) Spalart and Yang method.

5.1. 2D

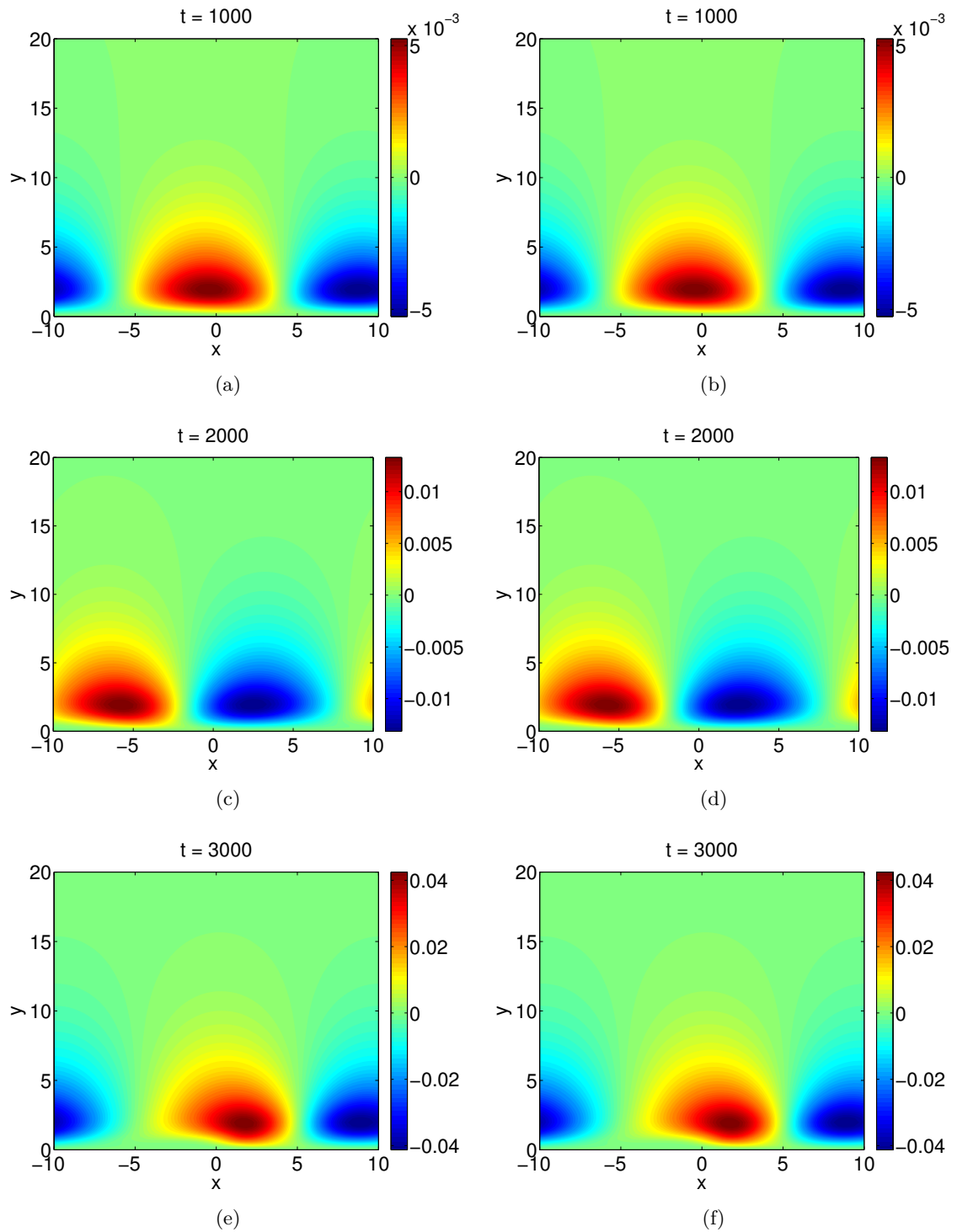


Figure 5.6: TS wave at time  $t = 1000, 2000$  and  $3000$  for  $R_{\delta^*} = 600$  showing increase in energy. (a), (c), (e) Present results; (b), (d), (f) Spalart and Yang method.

Though the flow fields look identical for both method in the figures 5.5 and 5.6, yet there is a difference in the solution of the flow. To check this we have produced the following figure by taking the norm of the element-wise difference of the solutions matrix in  $xy$ -plane for the six flow fields depicted in Figures 5.5 and 5.6 along with flow fields at time  $t = 5000$  and  $10000$ .

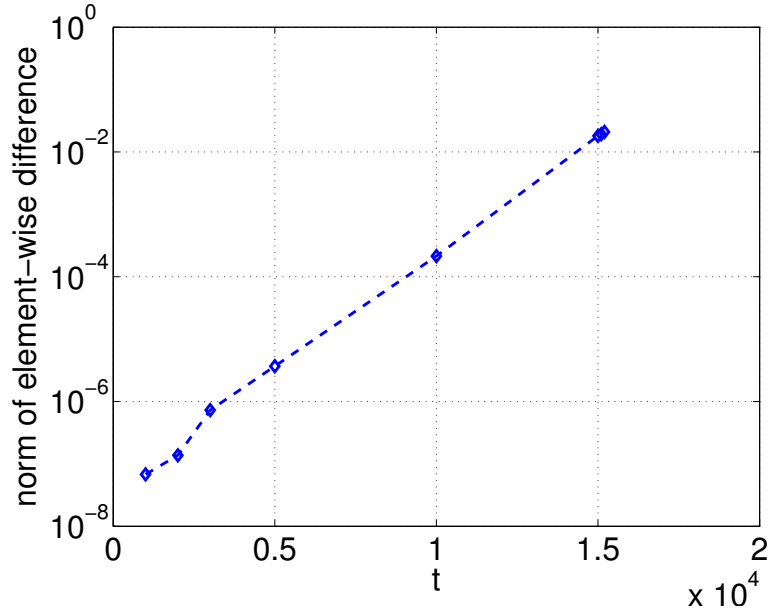


Figure 5.7:  $\log$ -plot of norm of the difference of the solutions of present results and Spalart and Yang method for eight flow fields at time  $t = 1000, 2000, 3000, 5000, 10000, 15100, 15200$  and  $15300$  for  $Re_{\delta^*} = 600$ .

Figure 5.7 shows the similar pattern as the figure 5.4(b) for  $Re_{\delta^*} = 600$ . Initially the norm of the difference of the solutions of two methods is almost zero and then increases as the time goes on.

Overall, in 2D case we have observed that for sub-critical Reynolds number the disturbance introduced to the flow field vanishes very quickly and both methods show almost same dynamics. On the other hand, for  $Re_{\delta^*} = 600$  two-dimensional TS waves never vanish from the flow fields rather it stays with almost constant energy (Figure 5.2(a)) for both methods. Two methods can be differentiated for  $Re_{\delta^*} = 600$  in term of TS waves energy as the energy is higher for present method, which is also reflected in the free-stream value in the Figure 5.3(b). This difference is because of the larger magnitude of the forcing for the present method. As the free-stream value is less than 1, the forcing magnitude for the present method would be larger than 1, while for the Spalart and Yang method which is 1 all the time.

## 5.2 3D

This section is devoted to the study of the development of the TS waves in a 3-dimensional domain. The associated number of spectral nodes in the  $x$ ,  $y$  and  $z$ -directions is  $(32 \times 65 \times 32)$ . One sub-critical ( $Re_{\delta^*} = 500$ ) and one super-critical ( $Re_{\delta^*} = 1000$ ) Reynolds number have been chosen to study the dynamics of the three-dimensional development of TS waves. The initial condition is the Blasius mean velocity profile disturbed by localized disturbance.

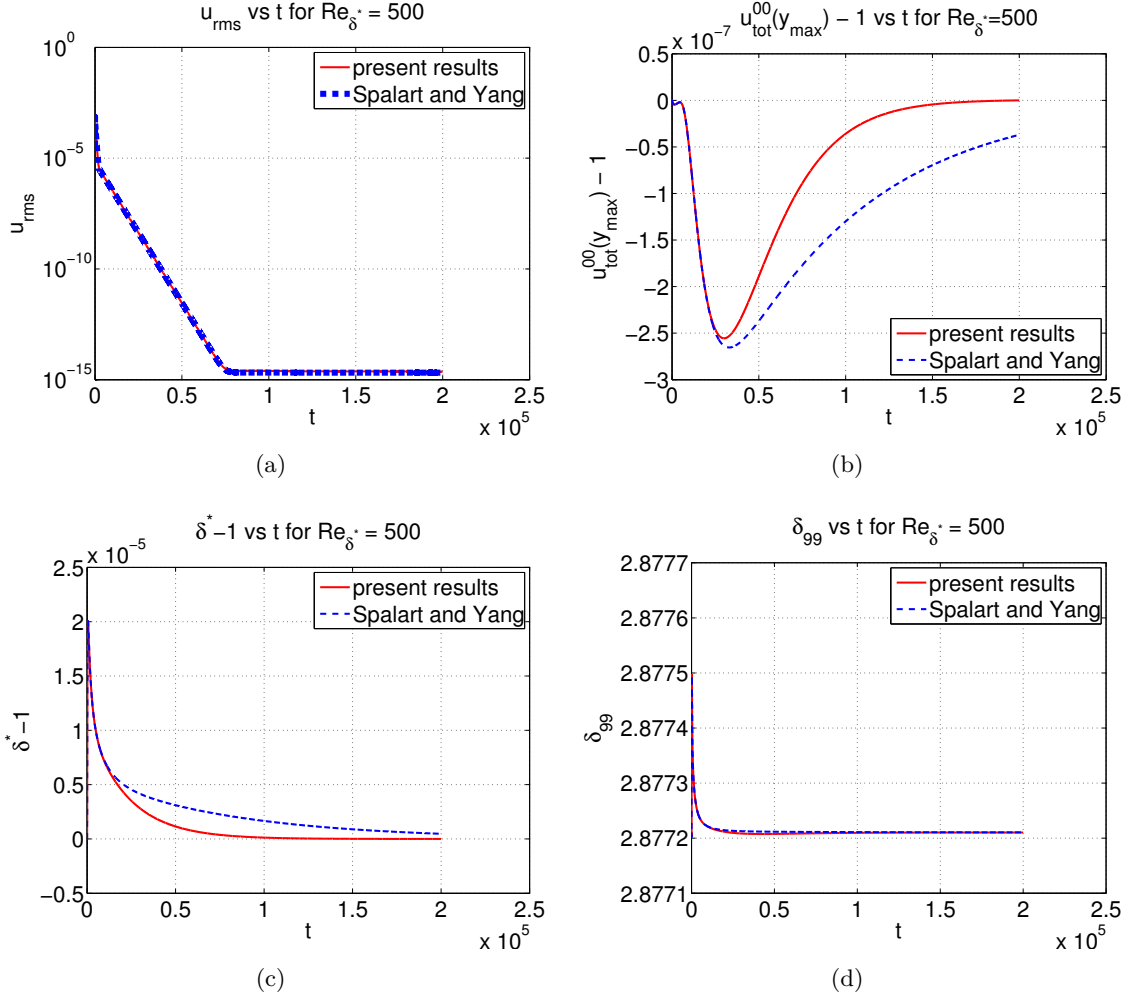


Figure 5.8: Comparing the results with Spalart and Yang method for  $Re_{\delta^*} = 500$  for a 3D domain. Figures shows the time evolution of (a)  $u_{rms}$ ; (b)  $u_{tot}^{00}(y_{max}) - 1$ ; (c)  $(\delta^* - 1)$  and (d)  $\delta_{99}$ .

Figure 5.8 indicates that for sub-critical Reynolds number  $Re_{\delta^*} = 500$ , the energy of the localized disturbance added to the Blasius profile, decreases rather fast as the advancement of time and the velocity profile clearly converges to the laminar Blasius profile for both the present result and Spalart and Yang method. Figure 5.9 shows that both methods retain the laminar Blasius profile after certain time period. The same behavior was observed for  $Re_{\delta^*} = 510$  in two-dimensional case.

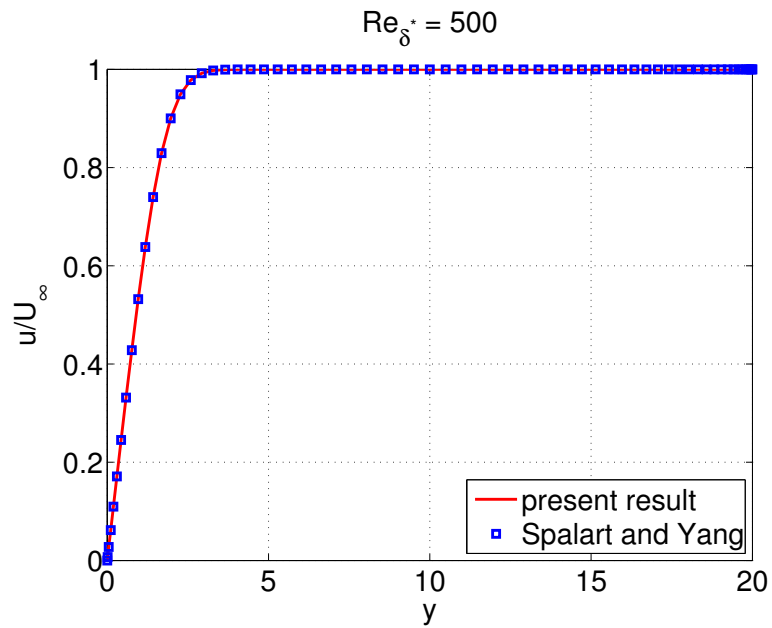


Figure 5.9: Mean-velocity profile non-dimensionalized by the local free-stream velocity  $U_\infty$  for  $Re_\delta^* = 500$  in 3D case. The figures was generated at  $x = 0$ ,  $z = 0$ .

Before wiping out completely the disturbance generates TS waves (Figure 5.10), which loses energy very quickly in the course of time to vanish from the flow. This energy decreasing of the TS waves is expected as in this case we are dealing with a Reynolds number less than the critical value 519.4. As we see in the Figure 5.10(d) for time  $t = 100000$ , the TS waves vanish from the flow as there is almost no disturbance in the flow. We just recover the initial flow profile.

5.2. 3D

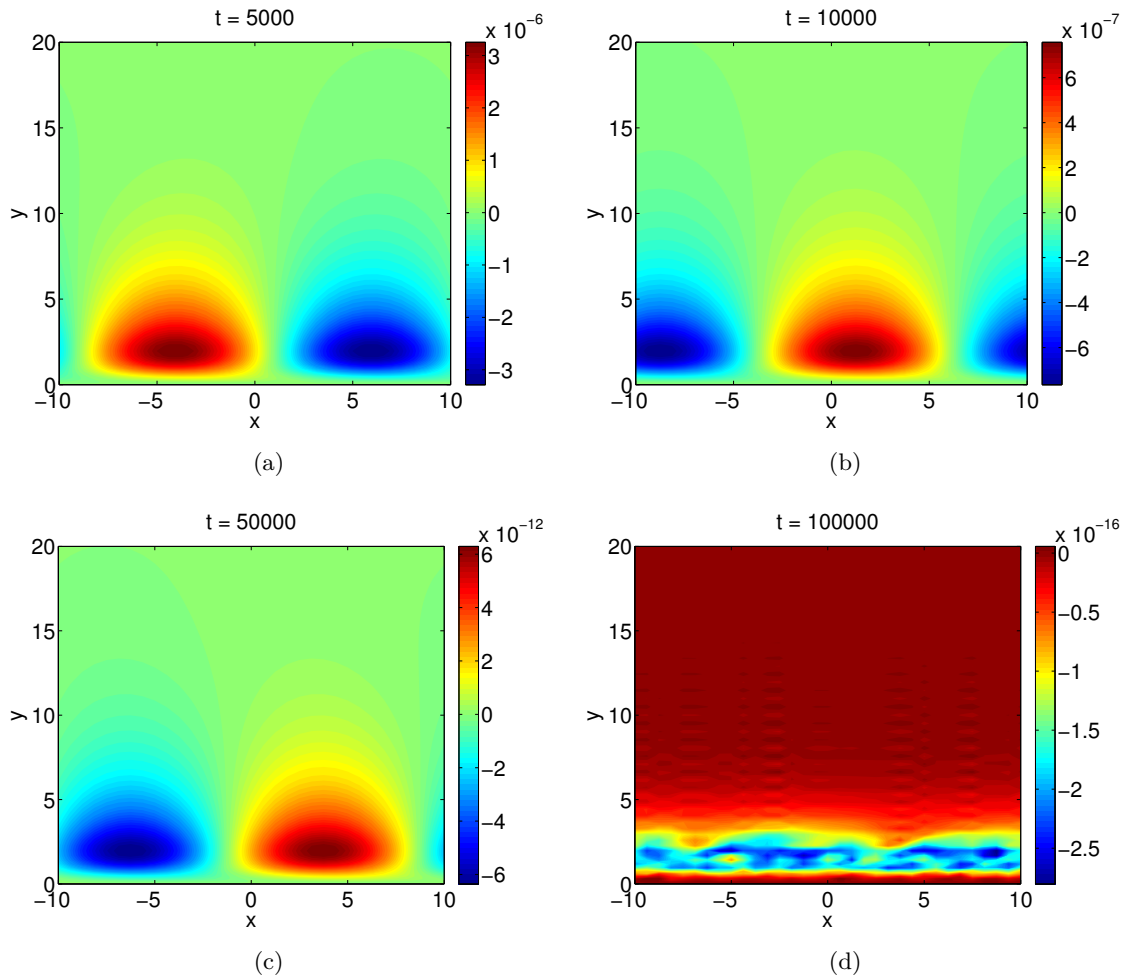


Figure 5.10: Generation of the TS waves in a 3D domain for  $Re_{\delta^*} = 500$  for the present study. Figures showing the evolution of TS waves at four instant of time (a)  $t = 5000$ ; (b)  $t = 10000$ ; (c)  $t = 50000$  and (d)  $t = 100000$ .

To understand the nature of the boundary-layer flow, i.e whether the flow is laminar or turbulent, one of the variables to study is shape factor defined by  $H = \frac{\delta^*}{\theta}$ , with the momentum thickness  $\theta = \int_{y=0}^{\infty} \frac{u}{U_{\infty}} (1 - \frac{u}{U_{\infty}}) dy$  is defined such that  $\rho U_{\infty}^2 \theta$  is the momentum loss in the actual flow because of the presence of the boundary layer. The standard laminar value for  $H$  is 2.59 while for the turbulence state it is 1.5. When breakdown occurs, the mean-velocity profile starts to lose Blasius shape and  $H$  shows clear signal to decrease from laminar value to its turbulence value and indicates the breakdown in the flow. In the following figure for shape factor  $H$  for  $Re_{\delta^*} = 500$  we see that the value of  $H$  is 2.59 throughout the whole simulation, means that the flow remains laminar during the simulation.

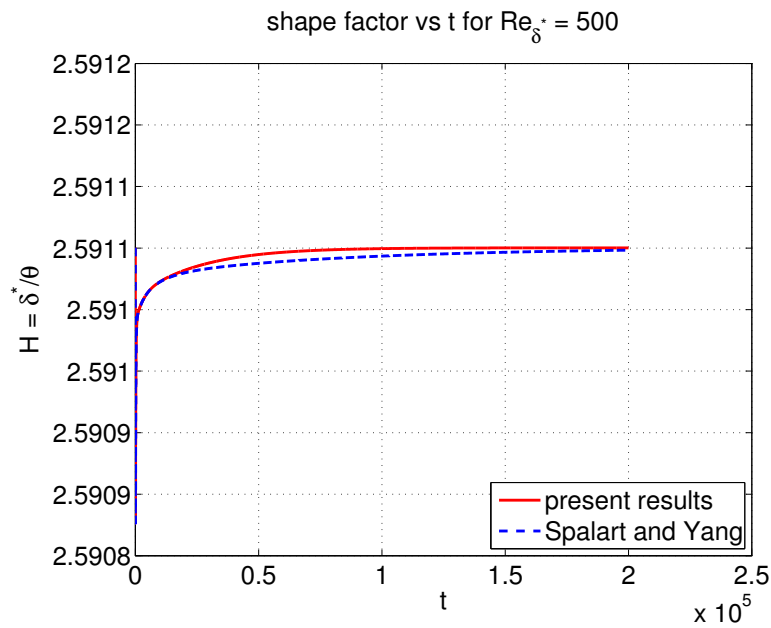


Figure 5.11: Shape factor  $H$  for  $Re_{\delta^*} = 500$  for both present and Spalart and Yang method. For both method the value of  $H$  is very close to the laminar value 2.59, indicating the laminar behavior of the flow throughout the simulation time.

5.2. 3D

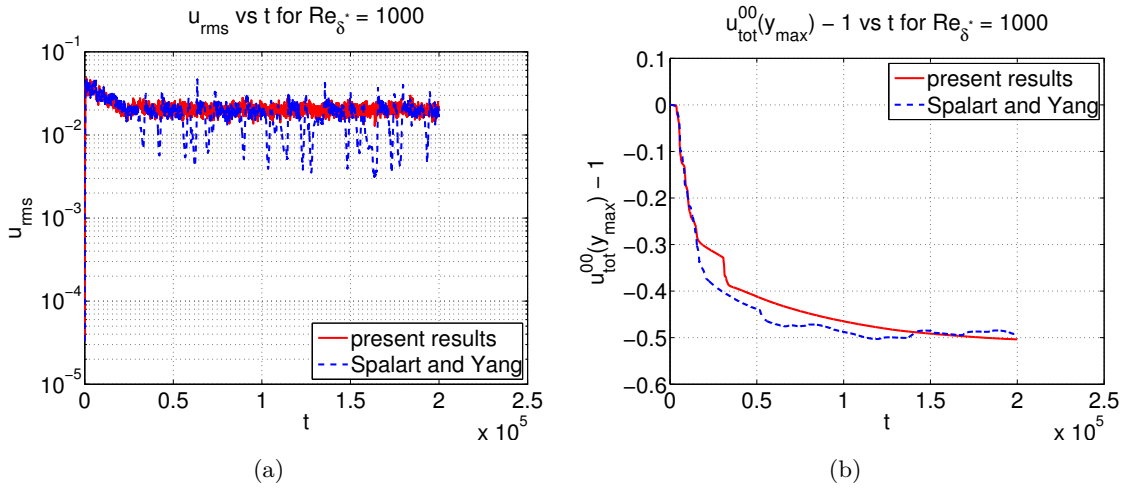


Figure 5.12: Comparing results with Spalart and Yang method for  $Re_{\delta^*} = 1000$  in 3D. Figures showing the time evolution of (a)  $u_{rms}$  and (b)  $u_{tot}^{00}(y_{max}) - 1$ .

We know that for Reynolds number larger than the critical value 519.4, the disturbance energy amplifies in time and the laminar state is no longer an attractor. In the figure 5.12(a), we can observe the amplification of the disturbance energy for  $Re_{\delta^*} = 1000$  for both methods. For the present method  $u_{rms}$  value contains almost constant and larger value compare to Spalart and Yang. Moreover, for Spalart and Yang case, the disturbance energy is fluctuating which results in the ups and downs of  $u_{tot}^{00}(y_{max})$  mode (Figure 5.12(b)). For both methods  $u_{tot}^{00}(y_{max})$  mode declines by 50% (Figure 5.12(b)) by the time  $t = 200000$  and shows clear intention of continuous declination for larger time period.

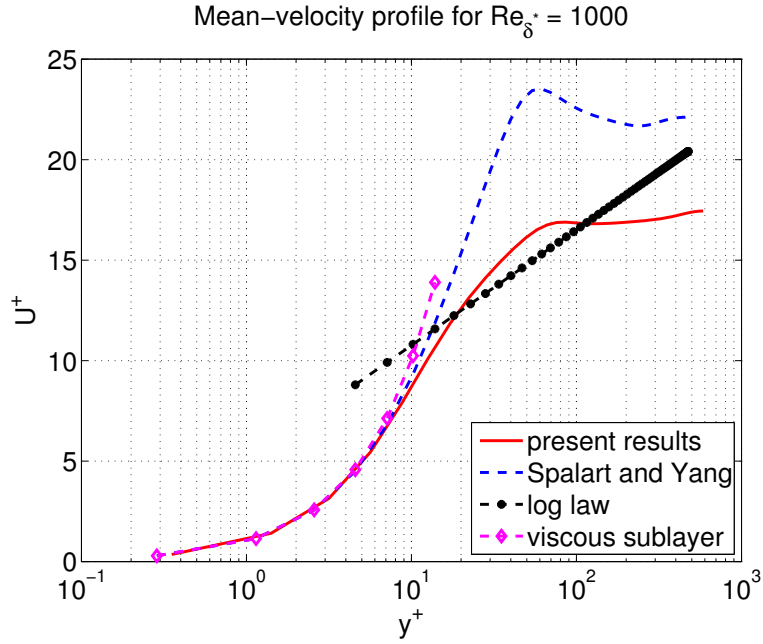


Figure 5.13: Mean-velocity profile using wall variables for  $Re_{\delta^*} = 1000$  in 3D case. The dotted lines represent the classical viscous sublayer  $y^+$  and the log law  $\kappa^{-1} \ln y^+ + C$ , where  $\kappa = 0.4$  and  $C=5$ .

Here,  $y^+$  is a non-dimensional wall distance for a wall-bounded flow defined by  $y^+ = \frac{u_\tau y}{\nu}$ , with  $u_\tau$  as friction velocity,  $y$  as the distance to the nearest wall and  $\nu$  as the kinematic viscosity of the fluid.

Figure 5.13 shows that both the present results and Spalart and Yang method are in good agreement in both the viscous sublayer  $y^+ < 5$  and the buffer layer ( $5 < y^+ < 30$ ). But in the log-layer starting at  $y^+ = 30$ , the agreement is not satisfactory with the turbulence flow for both methods, as the curves are higher for both methods in that region. Two methods also are not in good agreement in the the wake region. For the present method  $U_\infty^+$ , freestream velocity non-dimensionalized by shear velocity  $u_\tau$  is around 17, whereas for the Spalart and Yang case the value is approximately 22.

In the following Figures 5.14 and 5.15 we compare the turbulent intensities of the present results in terms of  $u_{rms}^+$ ,  $v_{rms}^+$ ,  $w_{rms}^+$  and  $(uv)^+$  for  $Re_\delta^* = 1000$  with Spalart and Yang method.

5.2. 3D

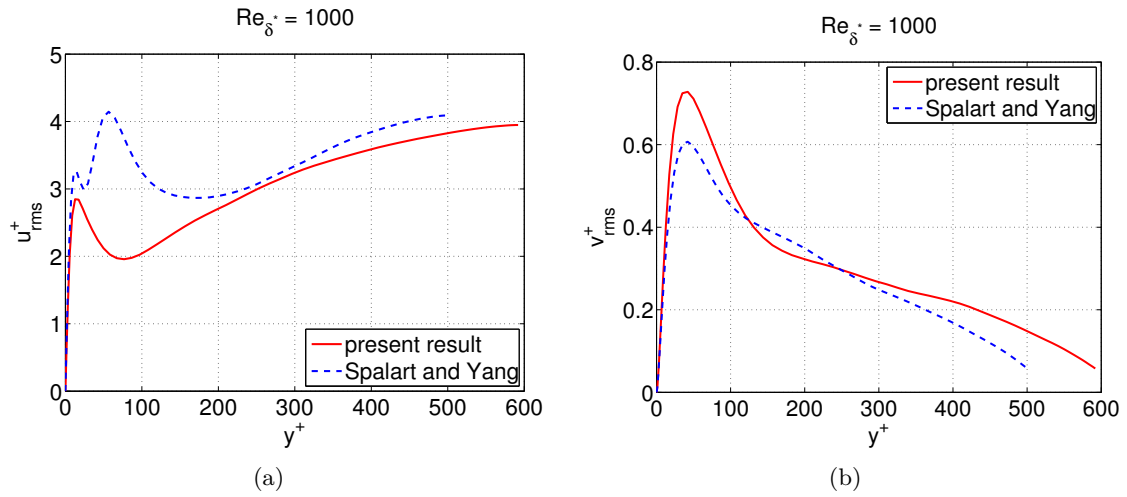


Figure 5.14: Comparing turbulent intensities in 3D domain with Spalart and Yang method for  $Re_{\delta^*} = 1000$ . (a)  $u_{rms}/u_{\tau}$ ; (b)  $v_{rms}/u_{\tau}$ .

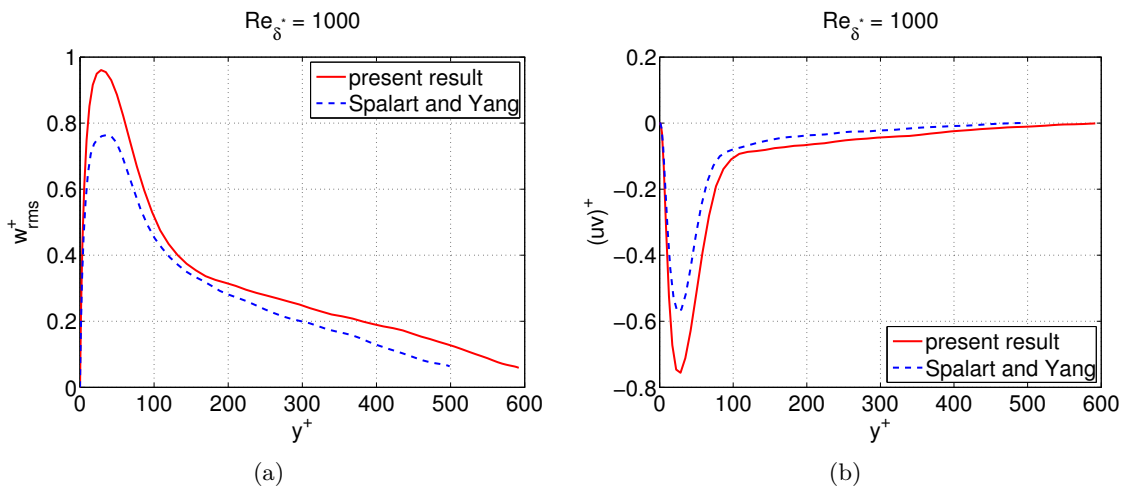


Figure 5.15: Comparing turbulent intensities in 3D domain with Spalart and Yang method for  $Re_{\delta^*} = 1000$ . (a)  $w_{rms}/u_{\tau}$ ; (b)  $uv/u_{\tau}$ .

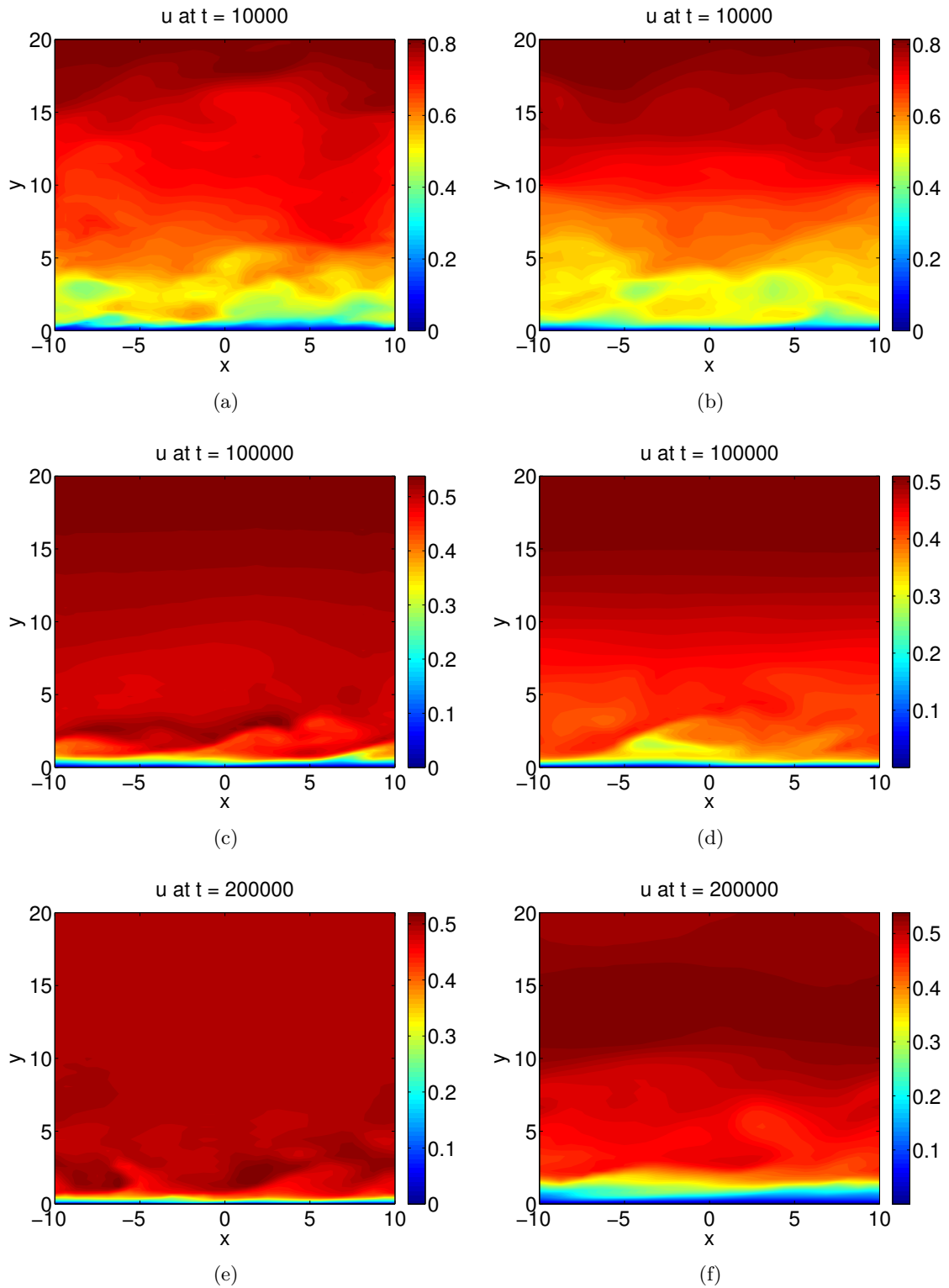


Figure 5.16: Visualization of the flow field for  $Re_{\delta^*} = 1000$  in terms of  $xy$ -contour plot of  $u$  at  $z = 0$  at three different instant of time  $t = 10000$ ,  $100000$ ,  $200000$ . (a), (c), (e) Present results; (b), (d), (f) Spalart and Yang method.

5.2. 3D

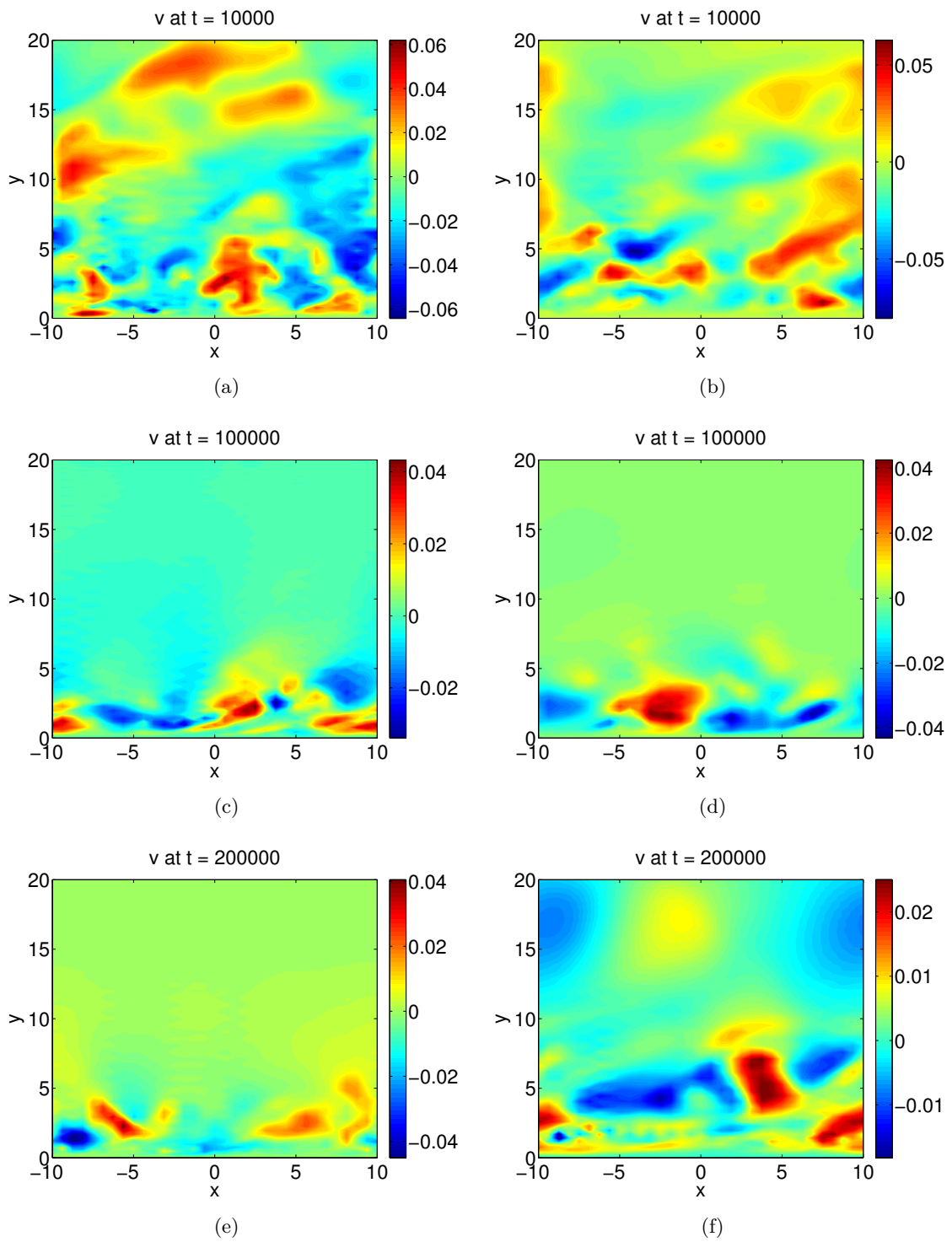


Figure 5.17: Visualization of the flow field for  $Re_{\delta^*} = 1000$  in terms of  $xy$ -contour plot of  $v$  at  $z = 0$  at three different instant of time  $t = 10000$ ,  $100000$ ,  $200000$ . (a), (c), (e) Present results; (b), (d), (f) Spalart and Yang method.

For further visualization of the flow field for  $Re_{\delta^*} = 1000$  we present in Figures 5.16 and 5.17, the  $xy$ -contour plot of instantaneous streamwise and normal velocity component  $u, v$  at three different instant of time. The presence of disturbance in the flow field results in positive and negative fluctuations both in  $u$  and  $v$  throughout the whole domain (Figures 5.16(a), 5.16(b), 5.17(a), 5.17(b)). But in the course of time larger fluctuations can be seen near the wall, which indicates the generation of elongated streamwise low and high speed streaks near the wall region. In Figure 5.20 we can see the positive and negative streamwise streaks in the flow field at four different instant of time for the present method. In the course of time, the streaks seems to vanish from the region far away form the wall, which is also quite clear from Figures 5.16(c) and 5.16(e). Similar behavior is observed for the  $v$  velocity component as the fluctuations far away from the wall seem to diminish in the course of time. For the present results the fluctuations in  $v$  seem to vanish in the free-stream for the larger time (Fig: 5.17(e)), but for the Spalart and Yang case the flow still experiences some fluctuations (Fig: 5.17(f)) in the free-stream.

5.2. 3D

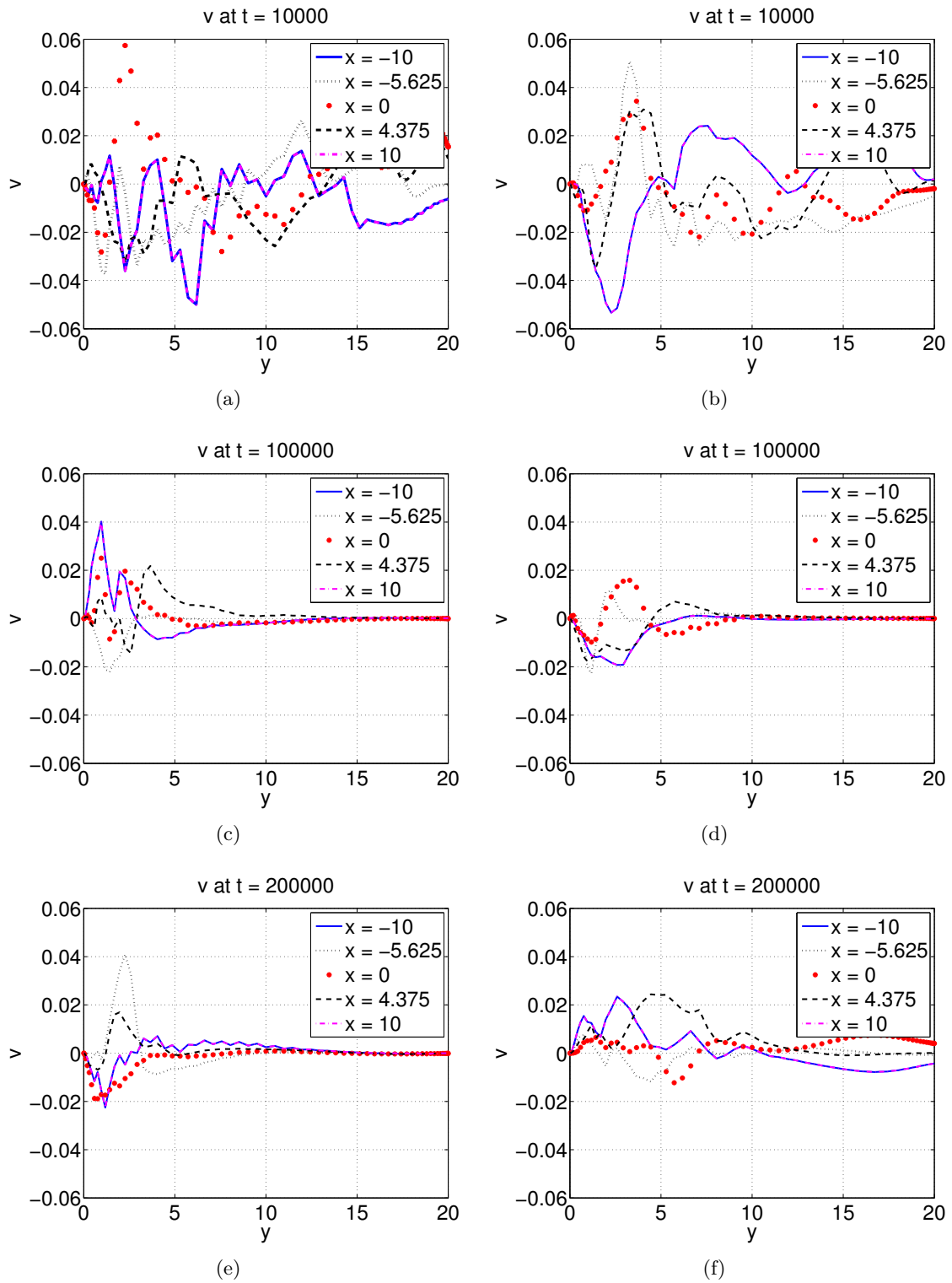


Figure 5.18:  $v$  vs  $y$  at five different points of  $x$  and  $z = 0$  in the flow field for three different instant of time  $t = 10000, 100000, 200000$ . (a), (c), (e) Present results; (b), (d), (f) Spalart and Yang method.

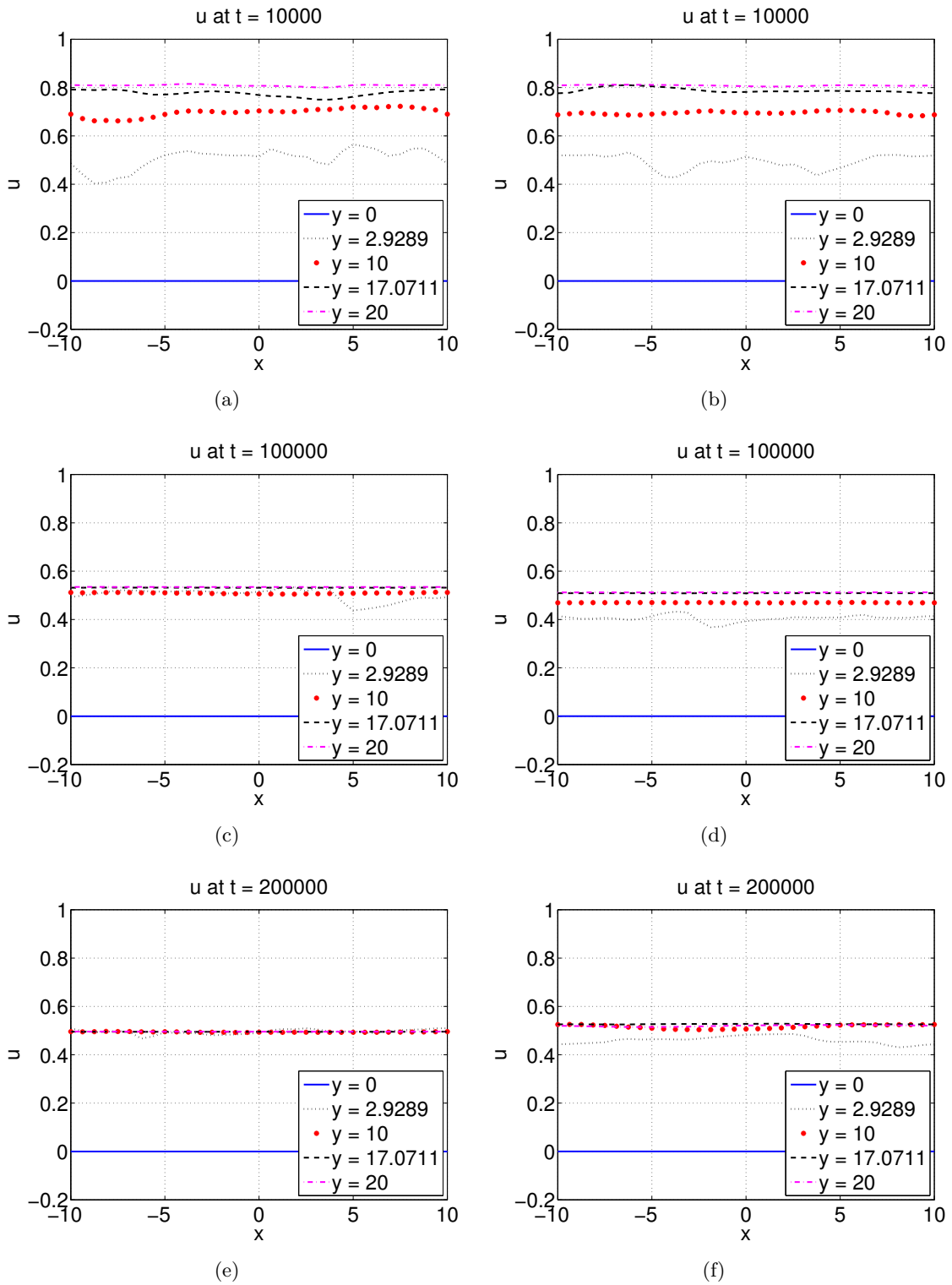


Figure 5.19:  $u$  vs  $x$  at five different points of  $y$  and  $z = 0$  in the flow field for three different instant of time  $t = 10000, 100000, 200000$ . (a), (c), (e) Present results; (b), (d), (f) Spalart and Yang method.

## 5.2. 3D

Figures in 5.18 and 5.19 clarifies the figures in 5.16 and 5.17 more precisely. As we see for the present method, the normal-velocity component (Figures 5.18(a), 5.18(c) and 5.18(e)) converges to 0 asymptotically near the edge of the domain in the advancement of time. Which precisely indicates that the flow becoming almost parallel near the edge (Figures 5.19(a),5.19(c) and 5.19(e)) after a longer period of time. But near the wall, after long time the flow still experiences the fluctuations both in  $u$  and  $v$  indicating the existence of the streaks and vortices. On the other hand, for the Spalart and Yang method, the normal velocity component does not converges to 0, at least for  $t = 200000$  (Fig: 5.18(f)) indicating the existence of turbulence not only near the wall but also far away from the wall.

Thus, we could say that for sub-critical Reynolds number  $Re_{\delta^*} = 500$  in 3D, both methods converge to the laminar state as they did in 2D case. One simple difference between two methods is that, for the present method mean velocity at the outer edge of the domain converges to laminar value 1 little faster than Spalart and Yang method ( Figure 5.8(b)). In contrast, for  $Re_{\delta^*} = 1000$ , present method attains better velocity profile and free-stream (Figure 5.13) and does not seem to have turbulence in the free-stream compare to Spalart and Yang by the time  $t = 200000$ . Moreover, for larger forcing amplitude present method maintains larger  $u_{rms}$  value than Spalart and Yang does.

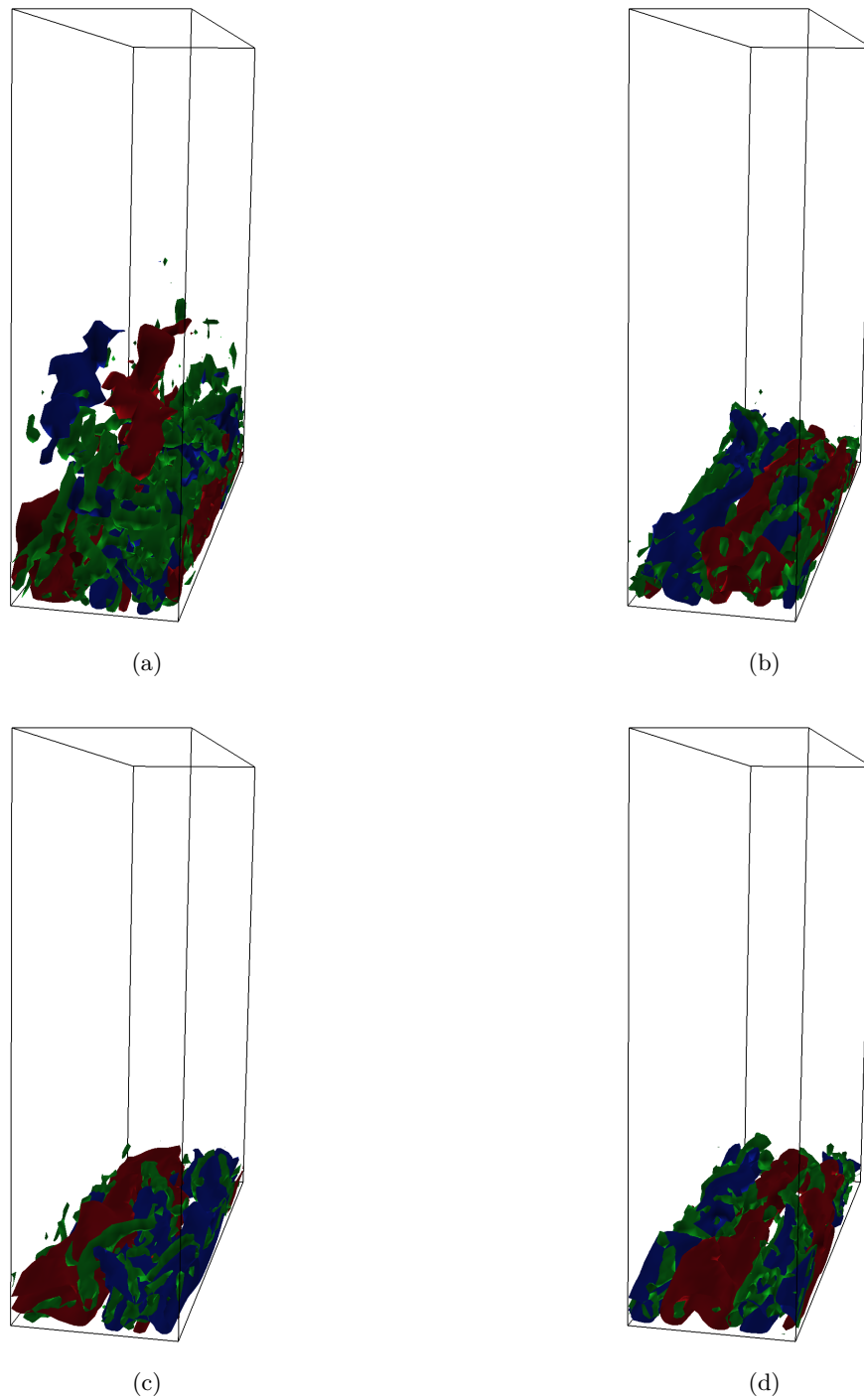


Figure 5.20: Snapshots of the turbulence structures near the wall for  $Re_{\delta^*} = 1000$  for the present method. Isosurfaces of streamwise velocity fluctuation  $u' = 0.05$  (high-speed streaks coloured in red),  $u' = -0.05$  (low-speed streaks coloured in blue) and  $\lambda_2 = -0.005$  (vortices coloured in green). Vortices are visualized using the  $\lambda_2$  criterion [10]. *a*)  $t = 10000$ ; *b*)  $t = 50000$ ; *c*)  $t = 100000$  and *d*)  $t = 200000$ .

### 5.3 Edge state

In this section the dynamics on the laminar-turbulent separatrix is investigated numerically for the boundary-layer flows in the subcritical regime. The number of spectral nodes in the  $x, y$ , and  $z$  was chosen to be  $(48 \times 97 \times 48)$ .

According to Schlichting (1987) [28], in case of spatially developing Blasius boundary layer, the laminar base flow is linearly stable for Reynolds number less than the critical value 519.4 based on displacement boundary layer thickness,  $\delta^*$ . However, subcritical transition may also occur in the presence of strong disturbances via the formation of streaks and vortices, bypassing the classical supercritical transition scenario [1]. These near-wall coherent structures such as streaks and quasi-streamwise vortices appear as a result of large sensitivity to forcing and large transient energy growth of these structures in shear flows [29]. Thus in the absence of any linear instability streamwise streaks and streamwise vortices can also be identified for boundary-layer flows and thus we have chosen  $Re_{\delta^*} = 500$  for tracking the edge state.

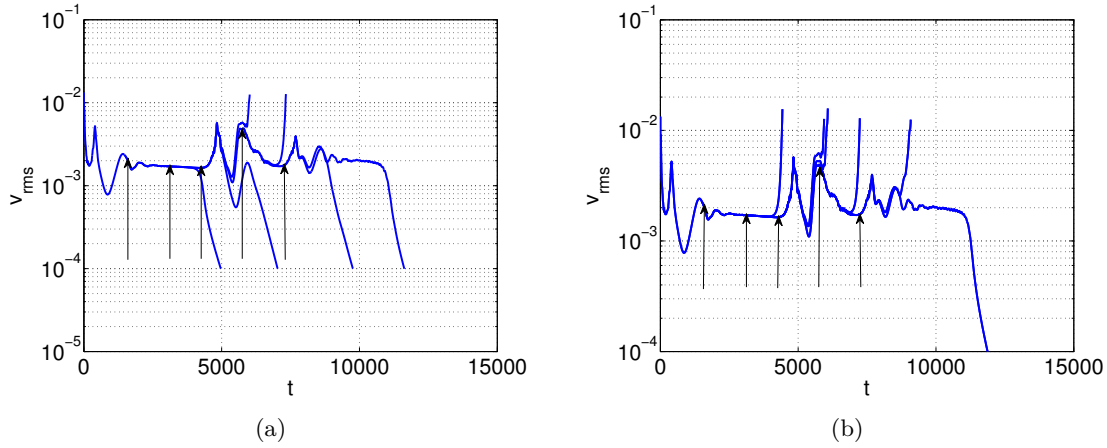


Figure 5.21: Root-mean-square (r.m.s) value of the wall-normal velocity fluctuations  $v_{rms}$ . Arrow signs represent the starting points of each refinement. (a) Presents results; (b) Spalart and Yang.

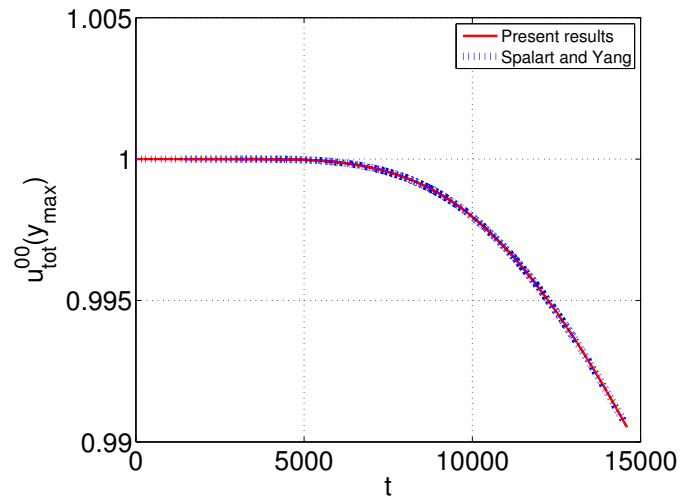


Figure 5.22: Time evolution of the mean velocity at  $y_{max}$  for both the present results and the Spalart and Yang method. For both cases  $u_{tot}^{00}(y_{max})$  decreases in time.

Figure 5.21 shows that both the present results and Spalart and Yang method follow the almost same laminar-turbulent trajectories at least upto time unit  $t = 10000$ . The mean velocity at the edge of the domain defined by the  $u_{tot}^{00}(y_{max})$  also quite same for both methods as we can see in the Figure 5.22.

As both methods exhibit almost same results, in the next page we present figures to visualize the laminar-turbulent separatrix for the present method only.

### 5.3. EDGE STATE

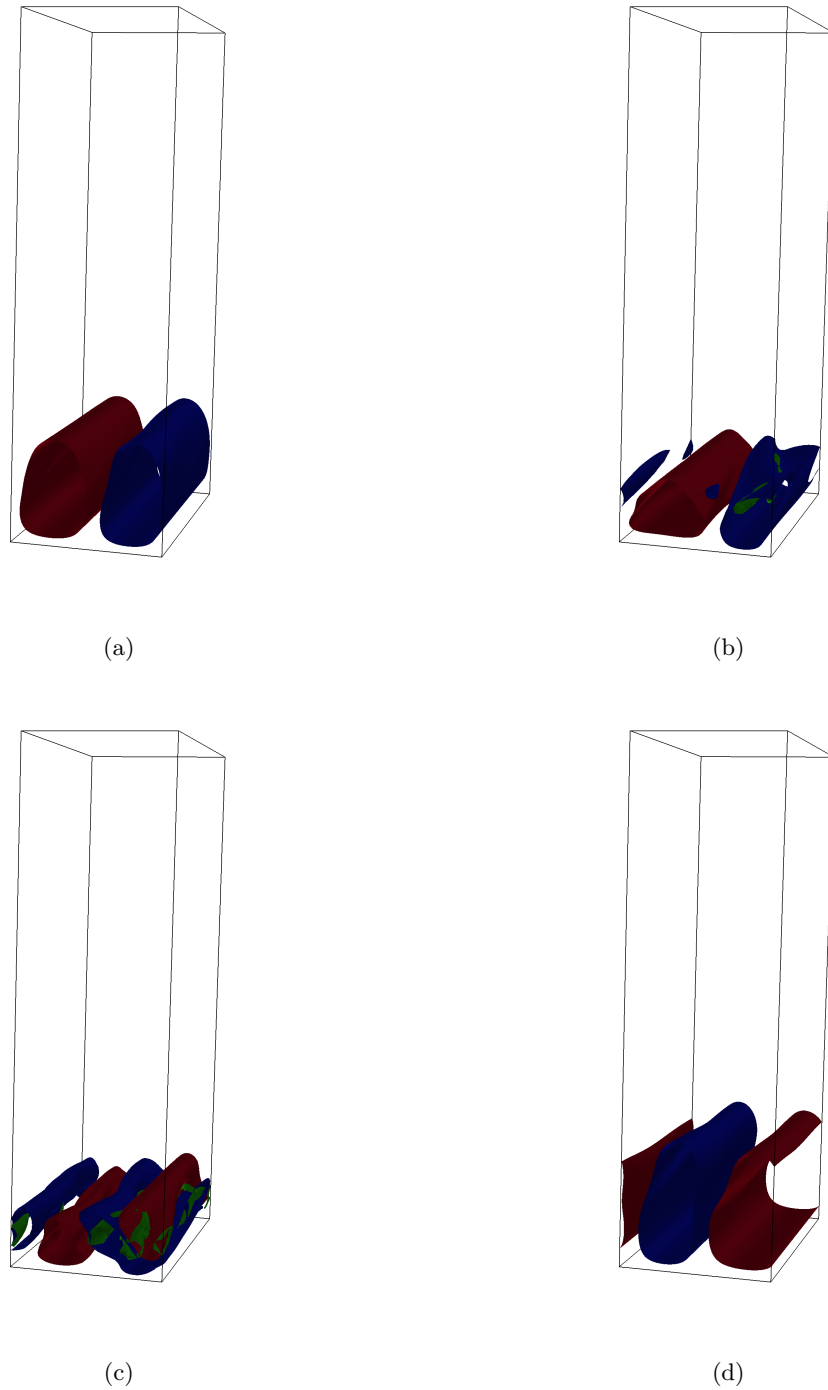


Figure 5.23: Three-dimensional visualization of the laminar-turbulent separatrix for  $Re_{\delta^*} = 500$  for the present method. Isosurfaces of streamwise velocity fluctuation  $u' = 0.05$  (high-speed streaks coloured in red),  $u' = -0.05$  (low-speed streaks coloured in blue) and  $\lambda_2 = -0.005$  (vortices coloured in green). Vortices are visualized using the  $\lambda_2$  criterion [10]. *a*) One high-speed streak with one low-speed streak at  $t = 900$ ; *b*) Generation of the strong quasi-streamwise vortices over the low-speed streak at  $t = 4600$ ; *c*) Breakdown at  $t = 4800$  and *d*) Regeneration of one high-speed streak with one low-speed streak with a shift in the position at  $t = 5400$ .

In the three-dimensional visualization of the laminar-turbulent separatrix in the Figure 5.23 we can see the calm phase at around  $t = 900$ . Then at around  $t = 4600$  strong quasi-streamwise vortices generated over the low-speed streak which grow in strength in time and wrap around the streak. The strengthen in the vortices induce upward motion that advects slow fluid away from the wall and finally results in breakdown at  $t = 4800$  and creates a high-speed streak in the position of the low-speed streak and low-speed streak shift it's position to the high-speed streak and the phase state becomes calm again at around  $t = 5400$ . We have observed the similar flow behavior for the larger time period.

## Chapter 6

# Conclusion and future work

In this study, we have modified the Navier-Stokes equations by an adapted forcing term on the assumption of parallel flow to keep the free-stream unperturbed and to ensure the correct development of the boundary-layer profile by combining the idea of Spalart and Yang [24] and Wedin *et al* [9]. The amplitude of the forcing term have been adapted based on the mean velocity at the outer edge of the domain. The idea was taken from Wedin *et al* [9], where they adapted the forcing term for the perturbation equations based on the mean flow at the edge of the domain defined as  $u_{tot}^{00}(y_{max})$ . But, in our study we have used adaptive forcing term for the total flow field. Having validating and comparing our results with Spalart and Yang method we have found slightly better results for the turbulence case, while for laminar case the results is almost similar to Spalart and Yang. But for finite amplitude disturbances and Reynolds number greater than the critical value 519.4, the present study fails to keep the free-stream unperturbed as the Spalart and Yang method does. In the last part, we have tried to identify the edge state and have found that for both methods the results is almost the same and the state is still chaotic for time units up to 10000. But because of computing time limitation we could not perform more refinements to reach to a possible periodic edge state. Thus, to achieve better result for the turbulence case one could use the iterative approach of computing the magnitude of the forcing term described in CHAPTER 3. For the edge state case, more refinement could be performed to check whether any of the methods reach a periodic state.



# Bibliography

- [1] Brandt, L., Schlatter, P. & Henningson, D.S. 2004 *Transition in boundary layers subject to free-stream turbulence* *J. Fluid Mech.* **517**, 167-198.
- [2] Craik, A.D.D. 1971 *Nonlinear resonant instability in boundary layers*. *J. Fluid Mech.* **50**, 393-413.
- [3] Damien Biau, *Laminar-turbulent separatrix in a boundary layer flow*. *Physics of fluids* **24**, 034107 (2012).
- [4] Ehrenstein, U. & Koch, W. 1995 *Homoclinic bifurcation in Blasius boundary-layer flow*. *Phys. Fluids* **7**, 1282-1291.
- [5] Ehrenstein, U. & Rossi, M. 1996 *Nonlinear Tollmein-Schlichting waves for a Blasius flow over compliant coatings*. *Phys. Fluids* **8**, 1036-1051.
- [6] Fasel, H. & Konzelmann, U. 1990 *Non-parallel stability of a flat-plate boundary layer using the complete Navier-Stokes equations*. *J. Fluid Mech.* **221**, 311-347.
- [7] Herbert, Th. 1984 *Analysis of the subharmonic route to transition*. AIAA-84-0009.
- [8] Herbert, Th. 1985 *Three-dimensional phenomena in the transitional flat-plate boundary layer*. AIAA-85-0489.
- [9] H. Wedin, A. Bottaro, A. Hanifi & G. Zampogna. *Recurrent unstable flow structures in the Blasius boundary layer*. *Eur. Phys. J.E (2014)* **37**: 34.
- [10] Jeong, J. & Hussain, F. 1995 *On the identification of a vortex*. *J. Fluid Mech.* **285**, 69-94.
- [11] Kachanov, Y.S. & Levchenko, V.Y. 1984 *The resonant interaction of disturbances at laminar-turbulent transition in a boundary layer*. *J. Fluid Mech.* **138**, 209-247.
- [12] Kline, S.J., Reynolds, W.C., Schraub, F.A. & Runstadler, P.W. 1967 *J. Fluid Mech.* **30**(4), 741-773.
- [13] Klingmann, G.B., Boiko, A.V., Westin, K.J.A., Kozlov, V.V. & Alfredsson, P.H. 1993 *Eur. J. Mech. B/Fluids* **12**, 493-514.
- [14] Koch, W. 1992 *On a degeneracy of temporal secondary instability modes in Blasius boundary-layer flow*. *J. Fluid Mech.* **243**, 319-351.
- [15] Koch, W., Bertolotti, F.P. & Hein, A. Stolte S. 2000 *J. Fluid Mech.* **406**, 131-174.
- [16] URL: [http://udel.edu/~inamdar/EGTE215/Laminar\\_turbulent.pdf](http://udel.edu/~inamdar/EGTE215/Laminar_turbulent.pdf).

- [17] Malik, M. R., Zang, T.A. & Hussaini, M.Y, 1985. *A spectral collocation method for the Navier-Stokes equations. J. Comp. Phys.*, **61**, 64-88.
- [18] Mattias Chevaller, Philipp Schlatter, Anders Lundbladh & Dan S. Henningson. *A Pseudo-Spectral Solver for Incompressible Boundary Layer Flows*. Technical Report, Stockholm, 2007.
- [19] Milinazzo, F.A. & Saffman, P.G. 1985 *Finite-amplitude steady waves in plane viscous shear flows. J.Fluid Mech.* **160**, 281-295.
- [20] Munson, B.R., Young, D.F., Okiishi, T.H. & Huebsch, W.W. 2010. *In Fundamentals of Fluid Mechanics, 6th Edition*. Wiley.
- [21] Muzycka, Y.S. & Yovanovich, M.M. 2010 *Unsteady viscous flows and Stokes first problem. International Journal of Thermal Sciences.* **49**, 820-828.
- [22] P.R. Spalart. 1984 *Numerical simulation of boundary-layer transition 9th Intl Conf. on Numerical Methods in Fluid Dynamics, Paris, June 25-29, 1984* (ed. S. Subbaramayer & J.P. Boujot), 531-535 Springer.
- [23] P.R. Spalart. 1998 *Direct numerical simulation of turbulent boundary layer up to  $Re_\theta = 1410$  , J. Fluid Mech.* **187**, 61-98 .
- [24] P.R. Spalart, Kyung-Soo Yang. 1987 *Numerical study of ribbon-induced transition in Blasius flow, J. Fluid Mech. vol.* **178**, 345-365.
- [25] Robinson, S.K. 1991 *Coherent motions in the turbulent boundary layer. Annu. Rev. Fluid Mech.* **23**, 601-639.
- [26] Rotenberry, J.M. 1993 *Finite amplitude steady waves in the Blasius boundary layer. Phys. Fluids A* **5**, 1840-1842.
- [27] Saric, W.S., Kozlov, V.V. & Levchenko, V.Y. 1984 *Forced and unforced subharmonic resonance in boundary-layer transition. AIAA* 84-0007.
- [28] Schlichting, H. 1987 *Boundary-layer theory, 7th edition*. McGraw-Hill.
- [29] Schmid, P.J. & Henningson, D.S. 2001 *2001 Stability and Transition in Shear Flows*. Springer.
- [30] Skufca, J.D., Yorke, J.A. & Eckhardt , B. 2006 *Edge of chaos in a parallel shear flows.. Phys. Rev. Lett.* **96**, 174101.
- [31] Smith, C.R. & Metzler, S.P. 1983 *The characteristics of low-speed streaks in the near-wall region of a turbulent boundary layer. J. Fluid Mech.* **129**, 27-54.
- [32] S.Toh & T. Itano. 2003 *A periodic-like solution in channel flow. J. Fluid Mech.* **481**, 67-76.
- [33] Taras Khapko. 2014. *Transition to turbulence in the asymptotic suction boundary layer*.
- [34] Thomas, A.S.W. 1983 *The control of boundary-layer transition using a wave-superposition principle. J. Fluid Mech.* **137**, 233-250.

- [35] URL: <http://encyclopedia2.thefreedictionary.com/boundary-layer+flow>.
- [36] Waleffe, F. 1997 *Exact coherent structures in turbulent shear flows*. *Phys. Fluids*, **9**, 883-900.
- [37] Wray, A. & Hussaini, M.Y. 1980 *Numerical experiments in boundary-layer stability*. *AIAA-80-0275* (see also *R. Soc. Lond. A* **392**, 373-389).





TRITA-MAT-E 2014:66  
ISRN-KTH/MAT/E—14/66-SE